Available online at www.sciencedirect.com

ScienceDirect

Geochimica et Cosmochimica Acta 127 (2014) 171–189

Geochimica et Cosmochimica Acta

www.elsevier.com/locate/gca

South Pacific dissolved Nd isotope compositions and rare earth element distributions: Water mass mixing versus biogeochemical cycling

Mario Molina-Kescher *, Martin Frank, Ed Hathorne

GEOMAR Helmholtz Centre for Ocean Research Kiel, Wischhofstraße 1-3, 24148 Kiel, Germany

Received 4 June 2013; accepted in revised form 26 November 2013; Available online 8 December 2013

Abstract

Despite its enormous extent and importance for global climate, the South Pacific has been poorly investigated in comparison to other regions with respect to chemical oceanography. Here we present the first detailed analysis of dissolved radiogenic Nd isotopes (ε_{Nd}) and rare earth elements (REEs) in intermediate and deep waters of the mid-latitude (~40°S) South Pacific along a meridional transect between South America and New Zealand. The goal of our study is to gain better insight into the distribution and mixing of water masses in the South Pacific and to evaluate the validity of Nd isotopes as a water mass tracer in this remote region of the ocean. The results demonstrate that biogeochemical cycling (scavenging processes in the Eastern Equatorial Pacific) and release of LREEs from the sediment clearly influence the distribution of the dissolved REE concentrations at certain locations. Nevertheless, the Nd isotope signatures clearly trace water masses including AAIW (Antarctic Intermediate Water) (average $\varepsilon_{Nd} = -8.2 \pm 0.3$), LCDW (Lower Circumpolar Deep Water) (average $\varepsilon_{Nd} = -8.3 \pm 0.3$), NPDW (North Pacific Deep Water) (average $\varepsilon_{Nd} = -5.9 \pm 0.3$), and the remnants of NADW (North Atlantic Deep Water) (average $\varepsilon_{Nd} = -9.7 \pm 0.3$). Filtered water samples taken from the sediment–water interface under the deep western boundary current off New Zealand suggest that boundary exchange processes are limited at this location and highlight the spatial and temporal variability of this process.

These data will serve as a basis for the paleoceanographic application of Nd isotopes in the South Pacific.

1. INTRODUCTION

The rare earth elements (REEs) are a coherent group of chemical elements (here the lanthanides and yttrium), for which the relative distribution or "pattern" is sensitive to oceanic processes such as scavenging and advection of water masses (e.g. Elderfield, 1988; Nozaki, 2001). The study of dissolved REEs in seawater has regained attention in recent years, in particular as a result of the use of Nd isotopes as a water mass tracer in oceanographic and paleoceanographic studies (e.g. Rickli et al., 2009; Roberts et al., 2010; Horikawa et al., 2011; Elderfield et al., 2012; Piotrowski et al., 2012; Martin et al., 2012; Stichel et al., 2012). This is possible because of the quasi-conservative behavior of Nd within distinct deep and intermediate water masses and due to the fact that Nd isotopes are not affected by biological fractionation (e.g. Frank, 2002; Goldstein and Hemming, 2003 and references therein). Studies based on Nd isotope compositions and REE distributions have helped to better understand present and past ocean circulation as well as weathering inputs and their relationship to climate on different time scales (e.g. Bertram and Elderfield, 1993; Piepgras and Jacobsen, 1992; Nozaki, 2001; Frank, 2002; Goldstein and Hemming, 2003; Scher and Martin, 2004; Lacan and Jeandel, 2005; Pahnke et al., 2008; Carter et al., 2012; Piotrowski et al., 2012; Singh et al., 2012).

* Corresponding author. Tel.: +49 431 600 2311.
E-mail address: mmolina-kescher@geomar.de (M. Molina-Kescher).

0016-7037/$ - see front matter © 2013 Elsevier Ltd. All rights reserved.
http://dx.doi.org/10.1016/j.gca.2013.11.038

The REEs can be divided into the light REEs (LREE) from La to Sm, the Middle REEs (MREE) from Eu to Dy, and the Heavy REEs (HREE) from Ho to Lu. Y behaves similarly to Ho because of the similar ionic radii (e.g. Nozaki, 2001). REE concentrations generally increase with water depth, similar to nutrients, as a consequence of particle scavenging in the surface and gradual remineralization of sinking particles, leading to REE release in deeper waters. Dissolved REEs fractionate coherently within the water column as a function of their ionic radii (e.g. Byrne and Kim, 1990). The LREEs are more particle reactive and therefore have shorter residence times than the HREEs, leading to differences in the REE profiles with water depth. Different water masses also present different absolute REE concentrations and ratios between REEs depending on the composition of their primary continental sources, as well as the age of a particular water mass or the scavenging intensity it has experienced. Cerium is exceptional in that it oxidizes to Ce(IV) in the water column thus becoming highly insoluble (Moffet, 1990). The main features of the shale-normalized patterns of seawater, which represent the fractionation of REEs with respect to the continental sources, are a gradual increase in abundance from the LREE to the HREE and a marked Ce depletion compared to its neighboring REEs (Elderfield, 1988; Byrne and Kim, 1990; Piepgras and Jacobsen, 1992; Nozaki, 2001 and references therein).

Radiogenic Nd isotope ratios ($^{143}Nd/^{144}Nd$) are generally expressed in the ε_{Nd} notation: $\varepsilon_{Nd} = [(^{143}Nd/^{144}Nd_{sample}/^{143}Nd/^{144}Nd_{CHUR}) - 1]^{*}10.000$, where CHUR stands for Chondritic Uniform Reservoir ($^{143}Nd/^{144}Nd = 0.512638$, Jacobsen and Wasserburg, 1980). Seawater acquires its dissolved Nd isotope signature through continental weathering either via riverine or dust input and via exchange with the continental margins (Lacan and Jeandel, 2005), which includes groundwater discharge (Johannesson and Burdige, 2007) and reactions with resuspended sediments (cf. Frank, 2002). Water masses originating from regions where young mantle derived material is weathered, such as around the Pacific Ocean, have higher, more radiogenic ε_{Nd} values, ranging from −2 to −4 in the North Pacific (Piepgras and Jacobsen, 1988; Amakawa et al., 2004, 2009). In contrast, contributions from old continental rocks result in more negative (unradiogenic) values. This is for example the case for the old cratonic rocks located in eastern Canada and northern Europe, which results in an ε_{Nd} value near −13 for North Atlantic Deep Water (NADW) (Piepgras and Wasserburg, 1987; Rickli et al., 2009). Those two most important end members mix within the Antarctic Circumpolar Current (ACC) resulting in intermediate present day ε_{Nd} values near −8.5 (Piepgras and Wasserburg, 1982; Stichel et al., 2012). A prerequisite for the use of ε_{Nd} signatures as water mass traces is the seawater residence time of Nd, which has been estimated to be between 300 and 1000 years (Tachikawa et al., 2003; Arsouze et al., 2009; Rempfer et al., 2011) and which is thus shorter than the global oceanic mixing time.

Nevertheless, the exact source and sink terms of Nd are still debated because of the apparent mismatch between Nd isotopes, which in the open ocean follow the advection and mixing of water masses, and Nd concentrations, which show a general increase with water depth and thus document vertical transport. This apparent contradiction has been named the Nd paradox (e.g. Goldstein and Hemming, 2003), which is most likely explained by reversible particle scavenging (Siddall et al., 2008), particularly in high productivity areas (e.g. Grasse et al., 2012) or near large river mouths (Singh et al., 2012). Another poorly understood aspect of marine Nd isotopes are the so-called boundary exchange processes that consider continental margins to be both an important source and sink of Nd in the oceans (Tachikawa et al., 2003; Lacan and Jeandel, 2005; Rempfer et al., 2011). These processes have been shown to change the isotope composition of Nd in seawater without significantly modifying its concentration (Lacan and Jeandel, 2005).

In the South Pacific the behavior of dissolved REE concentrations and Nd isotope compositions have not been systematically investigated until now. As pointed out in a recent global seawater Nd isotope compilation (Lacan et al., 2012) there is a general lack of data in the entire Pacific, in particular south of 30°S. Recent studies have contributed the first seawater Nd isotope data from the Pacific sector of the Southern Ocean and the Drake Passage (Carter et al., 2012; Stichel et al., 2012), as well as from the western (Grenier et al., 2013) and eastern equatorial Pacific (Grasse et al., 2012; Jeandel et al., 2013) but there are still only very few data for the large South Pacific basin.

The goal of this study is to better understand the behavior of dissolved REEs and Nd isotopes and their applicability as water mass tracers in the mid-latitude South Pacific. The South Pacific plays an important role for the global ocean circulation given that it represents the entrance and exit area for all deep waters of the largest ocean basin. We aim to elucidate the main factors controlling the distribution of REEs and Nd isotopes including advection, biogeochemical processes (scavenging), and boundary exchange processes. Although consisting of only 24 samples, this study covers the most important water masses in the southern Pacific and provides the first systematic evaluation of ε_{Nd} signatures and REE concentrations in this area, which will also serve as an important basis for reconstructions of past ocean circulation in the southern Pacific using Nd isotopes (e.g. Basak et al., 2010; Elderfield et al., 2012; Noble et al., 2013).

1.1. Hydrography and water column properties

Our study focuses on the body of water between New Zealand and South America between 35° and 50°S (Fig. 1a), the hydrography of which is dominated by waters originating from the Antarctic Circumpolar Current (ACC). A number of oceanographic studies have taken place in this remote region, many of them building on the knowledge acquired along longitudinal sections during the pioneering SCORPIO expeditions in the late 1960s (Stommel et al., 1973) and the more recent World Ocean Circulation Experiment (WOCE). One of the main features observed is a general southward flow of water masses between 1000 and 3500 m depth that are ultimately entrained

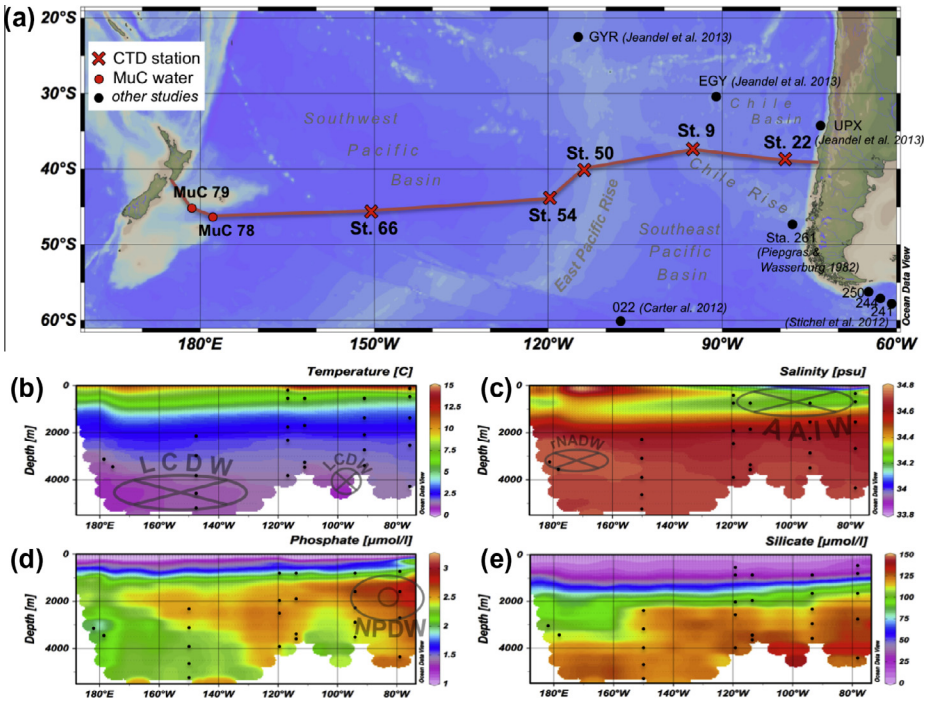

Fig. 1. Cruise track and locations of water sampling stations of expedition SO213 together with the most important hydrological properties (Data from the World Ocean Atlas 09). (a) Sampled locations: red crosses represent full depth CTD profiles and red dots represent bottom water samples obtained with a Multicorer (MuC). Black dots represent locations from other studies cited in the text. The most important bathymetric features are also indicated. The hydrological properties along the cruise track (red line) are provided in (b) Temperature (°C), (c) Salinity (psu), (d) Phosphate (µmol/l), (e) Silicate (µmol/l). Oxygen (ml/l) is presented in Fig. 5. The flow directions of the waters masses are also shown by transparent circles on the section plots of the properties, whereby crosses represent the sense of movement into the page and centred circles represent movement out of the page. Specific water masses are illustrated in the section plots according to hydrographic properties that allow their identification. Water mass abbreviations: LCDW (Lower Circumpolar Deep Water), rNADW (residual North Atlantic Deep Water), AAIW (Antarctic Intermediate Water) and NPDW (North Pacific Deep Water). Small black dots on the sections indicate the locations of the samples of this study. (For interpretation of the references to colour in this figure legend, the reader is referred to the web version of this article.)

in circumpolar waters of the ACC (Reid, 1973, 1986, 1997; Warren, 1973; Tsuchiya and Talley, 1996, 1999; Tsimplis et al., 1998; Wijffels, 2001). This flow is compensated by ACC derived northward moving water masses above and below.

The ACC is composed of deep waters admixed from the three major ocean basins, which results in the formation of Circumpolar Deep Water (CDW). The southeast Pacific sector of the Southern Ocean is also where equatorward flowing Antarctic Intermediate Water (AAIW) forms (Bostock et al., 2010) by winter air-sea exchange and cooling of Antarctic Surface Water (AASW) resulting in denser Subantarctic Mode Water (SAMW), which through further cooling is converted into AAIW (Sloyan and Rintoul, 2001). These fresh, oxygen-rich water masses occupy the depth range of 200 to 1500 m in the South Pacific and are transported along the anticyclonic pathway of the subtropical gyre, thereby ventilating the lower subtropical thermocline. Modified SAMW/AAIW returns poleward at the western boundary of the South Pacific and joins the AAC close to New Zealand near 170°W, 45°S.

Mixing with North Atlantic Deep Water (NADW) in the Atlantic sector of the Southern Ocean changes the properties of the upper part of CDW and thus divides it into Upper Circumpolar Deep Water (UCDW) and Lower Circumpolar Deep Water (LCDW). Nevertheless, the influence of NADW admixed in the Atlantic sector is still detectable in the western South Pacific between 180°E and 160°W by its salinity maximum and low nutrient concentrations near 3000 m (Fig 1c) (Reid and Lynn, 1971).

LCDW dominates the deeper water column flowing equatorward across the Southwest Pacific Basin (Fig 1b). It develops a deep western boundary current in its westernmost sector, which is considered responsible for the ventilation of the deep Pacific (Stommel and Arons, 1960; Reid et al., 1968). This is a consequence of the high oxygen content that LCDW acquires through admixture of one of its main sources, the Antarctic Bottom Water (AABW), which forms by sinking around Antarctica (Warren, 1973; Mantyla and Reid, 1983; Orsi et al., 1999). There is a strong vertical mixing component that tends to homogenize the hydrographic properties of LCDW characterized by low temperature, high salinity and high oxygen concentrations within the ACC.

UCDW enters the South Pacific near 120°W (Kawabe and Fujio, 2010) and its composition differs from that of LCDW mainly in its lower oxygen content, which originates from previous mixing with Indian Ocean deep waters

(Callahan, 1972). However, in the depth range of UCDW in the South Pacific (1500–3500 m) O_2 concentrations of UCDW are still higher than those of the water masses originating from the North Pacific and therefore UCDW is difficult to unambiguously identify by its hydrographic properties in our study area.

Mid-depth southward flow mainly occurs close to the South American continent in the form of North Pacific Deep Water (NPDW) (Fig. 1d and e), the precursors of which are ultimately LCDW and UCDW (Kawabe and Fujio, 2010). However, the original properties of those waters masses have been strongly modified during advection through the entire Pacific Ocean. The LCDW and UCDW become enriched in nutrients and depleted in oxygen due to respiration and remineralisation processes of organic matter as the water masses age. As a consequence, these waters are transformed into NPDW long before returning to the Southern Ocean (Shaffer et al., 2004; Wijffels, 2001; Kawabe and Fujio, 2010). Mid-depth waters with central Pacific characteristics are detectable by their lower [O_2] in the Southwest Pacific basin between 1500 and 3500 m depth (Fig 1d). This water body, from hereon referred to as South Pacific Gyre derived Deep Water (SPGDW), is the result of the mixing between UCDW that enters the South Pacific flowing across the East Pacific Rise and mid-depth central Pacific waters as a consequence of the middepths dynamics of the South Pacific Gyre (Reid, 1986), which supplies these less oxygenated waters in addition to pure UCDW to our study area.

The absence of deep water formation with characteristic hydrographic fingerprints in the North Pacific results in small differences of salinity and temperature in deep and intermediate waters throughout the Pacific. In the case of the South Pacific it is thus often difficult to distinguish northern and southern derived mid-depth water masses based on their hydrographic properties. In contrast, oxygen concentrations show marked differences between waters of northern and southern origin as a consequence of respiration during transport and aging of water masses. Oxygen concentrations are therefore a more suitable tool to distinguish waters from these sources and to track the return flow of mid-depth waters to the Southern Ocean.

2. SAMPLES AND METHODS

For this study, 26 seawater samples from depths between 300 and 5150 m were collected for analysis of REE concentrations and Nd isotope ratios along a longitudinal transect between 36°S and 45°S extending over approximately 10,000 km from central Chile to New Zealand (Fig. 1a). Samples were collected during Expedition SO213 of the German RV SONNE, which consisted of two legs from December 2010 to March 2011.

2.1. Sample collection

24 samples were collected from 5 profiles consisting of 4 to 5 depths using Niskin bottles attached to a CTD-rosette, which allowed the recovery of a volume of 18 to 20 l of seawater for every sample. The five bottom water samples obtained with the CTD-rosette were collected at approximately 2 m above the seafloor. In addition, off New Zealand 2 bottom water samples were recovered using a multicorer device (MuC) for the extraction of short undisturbed surface sediment cores that also allows the collection of bottom water immediately above the sediment–water interface (e.g. Haley et al., 2004). This water collected in the tubes of the device was carefully extracted without suspending the sediment and was subsequently filtered and treated in the same way as the other seawater samples. This method allowed the collection of about 10 l of bottom water for each of the two samples and enables the investigation of boundary exchange processes. Unfortunately this sampling method does not allow the acquisition of in situ hydrological properties, which were thus inferred from the World Ocean Atlas 2009 (WOA 09) (Fig. 1, Table 1).

2.2. Analytical procedures

All samples were filtered through 0.45 μm filters (nitrocellulose acetate) and were acidified to pH ~2.2 within the first two hours after collection. The majority of the water volume of every sample was used for the determination of the Nd isotope compositions but an aliquot of 0.5 to 2 litres of the same samples was separated for the determination of REE concentrations.

2.2.1. Determination of Nd isotope compositions and Nd concentrations by isotope dilution

The procedure applied for the extraction and isolation of the dissolved Nd is based on Fe co-precipitation of the REEs and was described in detail by Stichel et al. (2012). Briefly, after discarding the supernatant the Nd in the FeO-OH-precipitate was separated from the other elements by four principal steps: Rinsing with deionized water for removal of major seawater ions, liquid–liquid extraction using diethyl ether for separation of the Fe, and a two step ion chromatographic purification of Nd: First the REEs are separated from other elements using Biorad® AG50 W-X12 resin (200–400 μm mesh-size, 0.8 mL resin bed resin) (Barrat et al., 1996) and then the Nd is separated from the other REEs using Eichchrom® Ln Spec resin (50–100 μm mesh-size, 2 mL resin bed)(Le Fevre and Pin, 2005).

For the determination of the dissolved Nd concentrations an isotope dilution (ID) method was applied as described in Stichel et al. (2012), in which $^{150}Nd/^{149}Sm$ spike is added to an aliquot (0.5 L) prior to subsequent treatment. The Nd preconcentration, also based on Fe co-precipitation, and subsequent purification with only a single chromatographic separation was applied for the purification of the Nd using a 1.4 ml resin bed of BIORAD® AG50 W-X8, 200–400 μm mesh-size.

A Nu plasma MC-ICPMS at GEOMAR was used for the determination for both $^{143}Nd/^{144}Nd$ ratios and ID Nd concentration measurements. Instrumental mass fractionation was corrected by applying an exponential fractionation law using a $^{146}Nd/^{144}Nd$ ratio of 0.7219. The initial concentrations of the samples in the solutions for isotopic analysis ranged between 70 and 120 ppb, which were first

Table 1
Nd concentrations, Nd isotope compositions (IC) with external reproducibilities (2σ) and hydrographic data presented from east to west.

	Depth (m)	[Nd] (pmol/kg)	Nd IC ε_{Nd}	Ext. reprod. 2sd	θ (°C)	Salinity PSU	σ_θ (kg/m^3)	[Oxygen] (ml/l)	[Phosphate] (mmol/l)	[Silicate] (mmol/l)
Stations										
St. 22 (SO213-22-2)	300	11.2	−7.5	0.3	5.19	34.25	26.87	3.46	1.70	14.42
39°12′S, 79°55′W	650	10.4	−8.2	0.4	2.69	34.54	27.15	5.17	2.45	79.44
4144 m depth	1500	12.9	−5.4	0.4	1.77	34.64	27.78	2.63	2.30	103.99
	2600	16.1	−5.8	0.3	1.37	34.68	28.01	3.26	2.19	109.91
	4142	21.0	−6.6	0.4	1.00	34.70	28.12	3.79	2.06	112.82
St. 9 (SO213-09-2)	750	11.4	−9.0	0.3	7.49	34.27	27.14	5.15	1.90	10.25
37°41′S, 95°28′W	1500	14.0	−6.4	0.3	5.13	34.23	27.74	2.70	1.75	12.53
3771 m depth	2200	18.9	−6.8	0.3	2.58	34.56	27.96	3.24	2.54	90.29
	2800	21.0	−8.5	0.2	1.51	34.66	28.05	3.55	2.34	113.40
	3769	39.1	−9.1	0.3	0.94	34.70	28.11	3.83	2.19	115.68
St. 50 (SO213-50-1)	770	11.2	−8.8	0.4	5.59	34.27	27.10	5.26	1.66	12.17
40°17′S, 114°26′W	1800	15.3	−8.3	0.2	2.12	34.61	27.88	3.64	2.29	79.83
3483 m depth	3380	23.2	−6.9	0.2	1.10	34.68	28.09	3.71	2.34	113.97
	3481	23.1	−6.9	0.3	1.09	34.68	28.09	3.72	2.19	113.70
St. 54 (SO213-54-2)	350	11.0	−7.9	0.3	7.10	34.37	26.94	5.63	1.29	5.29
43°42′S, 120°30′W	800	9.7	−7.8	0.4	5.57	34.28	27.11	5.09	1.70	14.32
3844 m depth	1900	14.1	−7.6	0.2	2.11	34.61	27.89	3.57	2.21	83.21
	2400	18.6	−6.9	0.2	1.59	34.66	28.00	3.43	2.22	106.47
	3842	25.9	−6.5	0.2	0.95	34.69	28.12	3.84	2.16	113.54
St. 66 (SO213-66-1)	2200	14.4	−6.0	0.2	1.96	34.63	27.92	3.32	2.31	98.06
45°23′S, 151°42′W	3000	17.7	−6.6	0.2	1.41	34.69	28.05	3.57	2.24	104.87
5157 m depth	3800	22.5	−8.3	0.3	0.89	34.72	28.15	4.16	2.11	102.09
	4500	30.0	−8.3	0.2	0.50	34.71	28.20	4.35	2.10	110.75
	5155	30.6	−8.3	0.3	0.44	34.71	28.21	4.37	2.07	111.48
Multicorer samples										
MuC – 78	3410	22.8	−9.0	0.3	1.1*	34.72*	28.12*	4.64*	2.06*	111.26*
46°15′S, 179°37′W										
MuC – 79	3144	21.9	−10.3	0.3	1.4*	34.73*	28.08*	4.53*	1.90*	103.53*
45°51′S, 179°34′E										

[Nd] correspond to isotope dilution (ID) measurements. Values marked with * correspond to data obtained from the World Ocean Atlas 09 (WOA 09).
θ = Potential temperature. σ_θ = Potential density. PSU = Practical Salinity Units.

measured in autosampler sessions with samples and standards diluted to 50 or 60 ppb allowing duplicate measurements. Some duplicates were considerably less concentrated (10–30 ppb) and were therefore measured in time resolved mode. Typical total ion beam intensities for samples and standards ranged from 1.5 to 9 V for different measurement sessions with the low voltages realized by time resolved measurements. The results of the Nd isotope measurements were normalized to the accepted value of 0.512115 for the JNdi-1 standard (Tanaka et al., 2000), which was measured every two to six samples during each session together with an in-house standard. Standards and samples were diluted to the same concentration resulting in standard deviations (external reproducibility) of repeated standard measurements that ranged between 0.2 and 0.4 εNd units (2σ) for the autosampler sessions and between 0.3 and 1 εNd units (2σ) for the time resolved measurements. All duplicate isotope analyses resulted in identical εNd values within these uncertainties, whereby the results presented in Table 1 correspond to those measurements with the lower uncertainties of the individual analyses. Blank corrections were not applied as the blanks for both Nd isotope compositions and concentrations averaged 14 pg, representing around 1% of the concentrations of the samples. The entire protocol to measure seawater Nd isotopes in our laboratory corresponds to the one intercalibrated as part of the international GEOTRACES program (van de Flierdt et al., 2012).

2.2.2. Determination of REE concentrations

REE concentrations were obtained using an online preconcentration (OP) ICP-MS technique modified from Hathorne et al. (2012). Aliquots of 8 mL of filtered and acidified seawater were analyzed using a "seaFAST" system (Elemental Scientific Inc.) coupled to an Agilent 7500ce ICP-MS. The improved technique applied here utilises artificial standards with REE patterns similar to seawater, which were prepared using a seawater matrix, from which all REEs had been removed by Fe co-precipitation (Hathorne et al., 2012). The external precision based on repeated measurement of GEOTRACES inter-calibration samples (van de Flierdt et al., 2012) in the course of this study is reported in table 2. These values are within the uncertainties of between 6% and 22% (2σ) of the measurements

Table 2
REE concentrations (pmol/l), Er/Nd ratios, Ce anomalies ($Ce/Ce^* = 2[Ce]/([La]+[Pr])$) and GEOTRACES inter-calibration measurements (BATS) for this study.

	Depth (m)	Y (pmol/kg)	La (pmol/kg)	Ce (pmol/kg)	Pr (pmol/kg)	Nd (pmol/kg)	Nd(ID) (pmol/kg)	Sm (pmol/kg)	Eu (pmol/kg)	Gd (pmol/kg)	Tb (pmol/kg)	Dy (pmol/kg)	Ho (pmol/kg)	Er (pmol/kg)	Tm (pmol/kg)	Yb (pmol/kg)	Lu (pmol/kg)	HREE/LREE (Er/Nd)	Ce anomaly Ce/Ce^*
Stations																			
St. 22(SO213-22-2)	300	115	16.9	8.25	2.32	10.7	11.2	1.87	0.45	2.79	0.46	3.43	1.00	3.27	0.54	3.92	0.56	0.29	1.29
39°12′S, 79°55′W	650	107	15.6	5.84	2.36	10.6	10.4	1.71	0.45	2.36	0.43	3.86	1.14	4.02	0.59	4.24	0.71	0.39	0.65
4144 m depth	1500	148	22.3	6.78	2.87	12.7	12.9	2.16	0.61	3.23	0.55	4.84	1.44	5.36	0.86	5.98	1.14	0.42	0.54
	2600	192	28.6	7.15	3.55	14.3	16.1	2.39	0.79	4.20	0.62	5.77	1.76	6.00	1.08	6.87	1.29	0.37	0.45
	4142	178	33.8	7.74	4.68	21.0	21.0	3.70	0.92	4.94	0.85	6.85	2.00	6.85	1.06	8.02	1.36	0.33	0.40
St. 9(SO213-09-2)	750	110	17.5	7.97	2.60	11.5	11.4	2.05	0.56	2.62	0.48	3.91	1.11	4.03	0.65	4.32	0.80	0.35	0.79
37°41′S, 95°28′W	1500	148	24.1	9.89	3.06	13.1	14.0	2.14	0.61	3.27	0.54	4.54	1.33	5.02	0.84	5.30	1.02	0.36	0.73
3771 m depth	2200	163	31.1	17.5	4.48	18.3	18.9	3.05	0.73	4.37	0.72	5.71	1.68	6.24	0.97	6.85	1.30	0.33	0.98
	2800	160	33.0	17.3	4.72	19.8	21.0	3.43	0.80	4.39	0.77	5.59	1.62	6.02	0.90	6.79	1.18	0.29	0.92
	3769	209	58.6	56.6	9.92	38.3	39.1	7.80	1.43	8.04	1.22	8.70	2.21	7.37	1.15	8.11	1.34	0.19	1.65
St. 50(SO213-50-1)	770	106	16.5	7.20	2.38	10.5	11.2	1.89	0.45	2.36	0.49	3.58	1.09	3.81	0.57	4.04	0.77	0.34	0.76
40°17′S, 114°26′W	1800	143	26.7	10.5	3.49	15.1	15.3	2.49	0.66	3.64	0.62	4.94	1.50	5.43	0.79	6.06	1.03	0.36	0.69
3483 m depth	3380	204	37.7	6.79	4.98	22.1	23.2	3.73	1.03	5.69	0.92	6.93	2.02	6.67	1.05	7.86	1.46	0.29	0.32
	3481	181	35.0	5.09	5.01	22.4	23.1	3.86	0.93	5.29	0.90	7.19	1.99	6.93	1.10	7.65	1.45	0.30	0.25
St. 54(SO213-54-2)	350	110	16.2	12.0	2.49	9.67	11.0	1.80	0.56	2.61	0.41	3.78	0.99	3.62	0.54	3.76	0.67	0.33	1.29
43°42′S, 120°30′W	800	106	15.9	4.86	2.16	9.55	9.7	1.77	0.48	2.49	0.47	3.77	1.05	3.79	0.59	3.96	0.72	0.39	0.54
3844 m depth	1900	141	23.2	5.10	2.99	13.2	14.1	2.39	0.56	3.30	0.56	4.54	1.40	5.06	0.80	5.92	1.03	0.36	0.39
	2400	176	31.6	10.3	3.95	17.2	18.6	2.72	0.70	4.28	0.71	5.92	1.71	5.87	0.88	6.95	1.25	0.32	0.58
	3842	188	39.5	5.22	5.72	25.9	25.9	4.58	1.16	6.13	1.05	7.89	2.21	7.40	1.19	8.06	1.48	0.29	0.23
St. 66*(SO213-66-1)*	2200	164	26.2	4.05	2.88	12.8	14.4	2.38	0.62	3.97	0.66	5.40	1.51	5.23	0.86	6.09	1.12	0.36	0.28
45°23′ S, 151°42′W	3000	151	29.4	8.67	3.70	16.3	17.7	2.55	0.60	3.51	0.60	5.03	1.59	5.79	0.88	7.13	1.23	0.33	0.52
5157 m depth	3800	164	34.3	5.24	4.86	22.3	22.5	3.98	1.00	4.86	0.86	6.64	1.91	6.24	0.95	6.83	1.30	0.28	0.27
	4500	204	46.7	11.5	6.98	28.0	30.0	5.66	1.22	7.04	1.01	7.92	2.12	7.14	1.15	7.31	1.37	0.24	0.43
	5155	178	41.7	6.53	6.47	29.5	30.6	5.63	1.22	-	1.23	8.10	2.06	7.08	1.07	7.54	1.39	0.23	0.27
Multicorer samples																			
MuC – 78	3410	166	36.5	15.1	5.15	20.7	22.8	3.92	0.95	4.91	0.77	6.36	1.75	6.04	0.96	6.70	1.09	0.26	0.73
46°15′S, 179°37′W																			
MuC – 79	3143	157	34.9	16.1	4.89	21.3	21.8	3.34	0.83	4.69	0.80	6.07	1.67	6.01	1.00	6.44	1.18	0.28	0.81
45°51′ S, 179°34′E																			

GEOTRACES BATS intercalibration:		Y (pmol/kg)	La (pmol/kg)	Ce (pmol/kg)	Pr (pmol/kg)	Nd (pmol/kg)	Sm (pmol/kg)	Eu (pmol/kg)	Gd (pmol/kg)	Tb (pmol/kg)	Dy (pmol/kg)	Ho (pmol/kg)	Er (pmol/kg)	Tm (pmol/kg)	Yb (pmol/kg)	Lu (pmol/kg)
BATS 2000 m																
Average:	*(n = 5)*	127	22.3	4.59	3.71	16.5	3.28	0.78	4.15	0.70	5.14	1.42	4.77	0.69	4.51	0.75
2σ:		16.3	1.44	2.86	0.32	0.76	0.31	0.09	0.73	0.07	0.46	0.11	0.27	0.05	0.36	0.05
BATS 15 m																
Average:	*(n = 5)*	124	14.1	10.8	2.97	13.6	2.91	0.79	4.38	0.77	5.42	1.40	4.53	0.67	4.19	0.65
2σ		16.8	1.64	2.89	0.18	0.84	0.30	0.06	0.54	0.06	0.64	0.14	0.44	0.04	0.30	0.09

[REE] correspond to OP-ICPMS measurements, whereby isotope dilution (ID) results for [Nd] are also shown. Er/Nd ratios were calculated using the more precise ID method for the Nd concentrations. See van de Flierdt et al. (2012) for GEOTRACES inter-calibration. See van de Flierdt et al. (2012) for GEOTRACES inter-calibration.

of the individual REEs (Hathorne et al., 2012) identical to the consensus values reported by van de Flierdt et al. (2012).

2.2.3. Determination of nutrient concentrations

Dissolved silicate and phosphate concentrations were measured at the Alfred Wegener Institute Bremerhaven following standard procedures (Grasshoff et al., 1999).

3. RESULTS

All the results presented in this study are available in the database of PANGAEA® (www.pangaea.de).

3.1. Hydrography at the sampling sites

The distribution of water masses described in the introduction is generally consistent with the hydrographic data obtained for the five full water depth profiles (Fig. 2). The similarity of the temperature-salinity characteristics of northern and southern derived deep waters requires the water mass characteristics in Fig. 2a to be defined by oxygen concentration against potential density (σ_θ). With this approach the major water masses present at our sampling sites can be distinguished with the exception of UCDW, which is more difficult to identify in some cases (e.g. St. 09) as it is essentially identical to Pacific-derived waters with the same density range.

Station 22 exhibits a marked O_2 minimum of 3.46 ml/l at 26.87 kg/m^3 sampled at 300 m depth indicating the presence of Equatorial SubSurface Water (ESSW) (Fig. 2a). In the potential density range from 26.9 to 27.3 kg/m^3 the low salinities and high O_2 concentrations mark the presence of SAMW and AAIW, which was sampled at all stations except station 66. Below this depth, there is a clear bifurcation to waters with oxygen concentrations as low as 2.6 ml/l in the easternmost profiles 22 and 9, reflecting the southward flow of NPDW. This difference disappears at around 28.0 kg/m^3, where all profiles converge again coinciding with the presence of Antarctic derived waters. Profile 22 remains slightly less oxygenated than the rest of the stations indicating a stronger Pacific influence at this location. Pure LCDW has only been sampled in the deepest of all five profiles at station 66 located in the central southwest Pacific basin. UCDW can be identified by its lower oxygen content (3.5 ml/l) and higher potential density with respect to LCDW and is least diluted in profiles 50 and 54 located above the East Pacific Rise, where the influence of water masses originating from the north is smaller but not absent. The presence of pure circumpolar deep waters (UCDW/LCDW) in the deepest part of profile 9 documented in the sections of Fig. 1 (data from the World Ocean Atlas 09), is not reflected in Fig. 2 because of the difficulty of distinguishing UCDW based on hydrographic data. In the density range of UCDW the lower [O_2] in profile 66 indicates the southward flow of central Pacific waters (SPGDW).

The nutrient profiles (Fig. 2b and c) show depleted concentrations for both silicate and phosphate in surface waters, which increase with depth. Nevertheless while

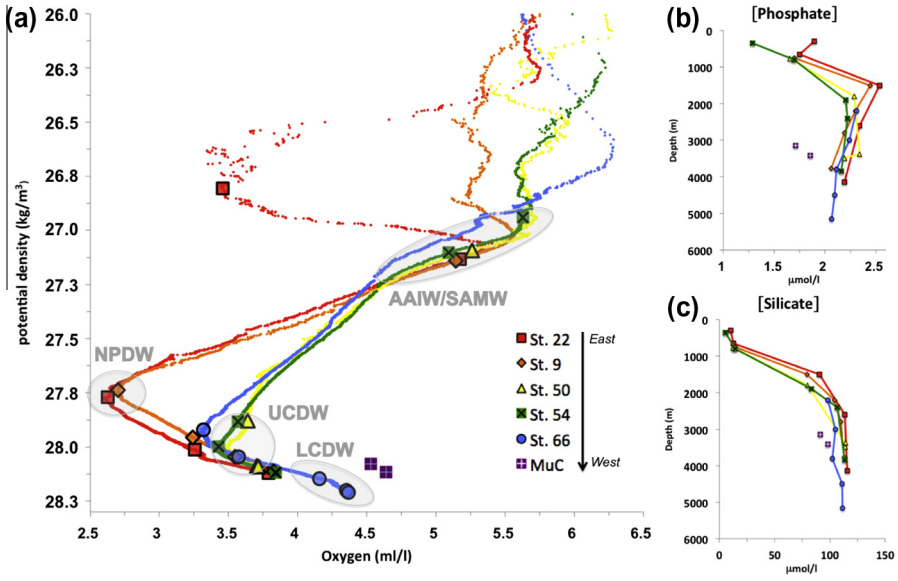

Fig. 2. (a) Potential density versus oxygen for the five CTD profiles and multicorer water samples (MuC) obtained during cruise SO213. From east to west: St. 22 (red), St. 9 (orange), St. 50 (yellow), St. 54 (green), St. 66 (blue) and MuC (purple). Data for the MuC samples were taken from the World Ocean Atlas 09 (WOA 09). The identified major water masses are indicated by grey circles: SAMW/AAIW (SubAntarctic Mode Water/Antarctic Intermediate Water), NPDW (North Pacific Deep Water), UCDW (Upper Circumpolar Deep Water) and LCDW (Lower Circumpolar Deep Water). Symbols represent the distinct water samples in the colours of their respective stations. (b) and (c) Phosphate and silicate concentrations versus depth in µmol/l for the five CTD profiles and the multicorer water samples (MuC). R. Tiedemann (AWI) provided the nutrient data, except for the data for the MuC samples, which were taken from WOA 09. (For interpretation of the references to colour in this figure legend, the reader is referred to the web version of this article.)

silicate concentrations reach their maxima in the bottom waters, phosphate maxima are present between 1500 and 3500, especially for samples 22–1500 (St. 22, 1500 m water depth) and 9–1500 (St. 9, 1500 m water depth) coinciding with the main core of NPDW.

Figs. 1c,e,f and 2b,c indicate that the two multicorer samples are located under the influence of the last remnant of NADW, as indicated by the high salinity and low nutrient content.

3.2. REE distribution

The REE concentrations, with the exception of Ce, (Fig. 3, Table 2) increase with water depth as expected for open ocean waters. The increase is generally linear with depth for the light and middle REEs, whereas for the heavier REEs the shape of the profiles gradually becomes more convex, similar to that of dissolved silicate concentrations (Fig. 2c) but significantly less pronounced. In contrast Ce concentrations show little systematic variation with water depth ranging between 5 and 17 pmol/kg. The only exception to the generally steady increase of dissolved REE concentrations with depth is the bottom sample of station 9 (9–3769), which shows anomalously high concentrations of all LREEs, in particular of Ce.

The REE patterns normalized to Post-Achaean Australian Sedimentary rocks (PAAS) (Taylor and McLennan, 1985) are presented in Fig. 4 and are generally typical for open ocean seawater samples. All patterns exhibit a negative Ce anomaly and a progressive enrichment from LREEs to HREEs that becomes more pronounced with water depth.

3.3. Nd concentrations

The Nd concentrations (Fig. 3, Tables 1 and 2) obtained by OP-ICP-MS (table 2) are on average 5%, lower than those obtained using the more precise Isotope Dilution (ID) technique (table 1) but identical within the 95% confidence limits of the technique (Table 2). The maximum difference between the techniques was 12% for sample 54–350, similar to previous considerations of its uncertainties (Hathorne et al., 2012).

Nd concentrations are nearly constant around 10 pmol/kg in the shallowest two samples (22–300 and 54–350) and at ~800 m depth. Below that Nd concentrations increase with depth at all stations. Excluding the anomalous maximum of sample 9–3769 (39 pmol/kg), the Nd concentrations of the bottom samples vary between 21 pmol/kg (st. 22) and 30.6 pmol/kg for the deepest sample (66–5155). The increase in profile 66 is steady until 4500 m depth (30 pmol/kg) but below only shows a small increase until 5155 m depth. The multicorer samples have dissolved Nd concentrations similar to other samples from similar

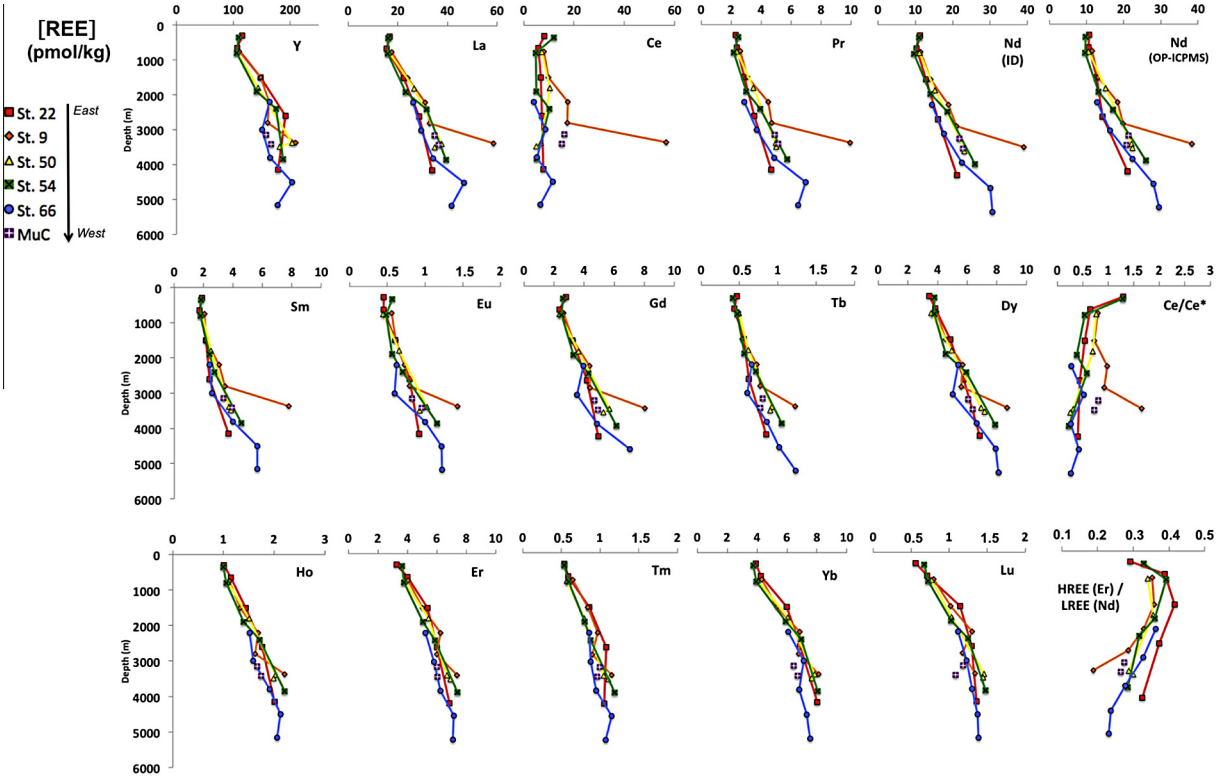

Fig. 3. REE concentrations (pmol/l), HREE/LREE (Er/Nd) ratios and Ce anomalies ($Ce/Ce^{*} = 2[Ce]/([La]+[Pr])$) versus water depth (m). Samples from the five CTD profiles and the two multicorer water samples (MuC) are presented, from east to west: St. 22 (red), St. 9 (orange), St. 50 (yellow), St. 54 (green), St. 66 (blue) and MuC (purple). All REE concentrations were obtained by OP-ICP-MS, while Nd concentrations were obtained by both isotope dilution (ID) and OP-ICP-MS. Er/Nd ratios were calculated using the more precise ID method for the Nd concentrations (For interpretation of the references to colour in this figure legend, the reader is referred to the web version of this article.).

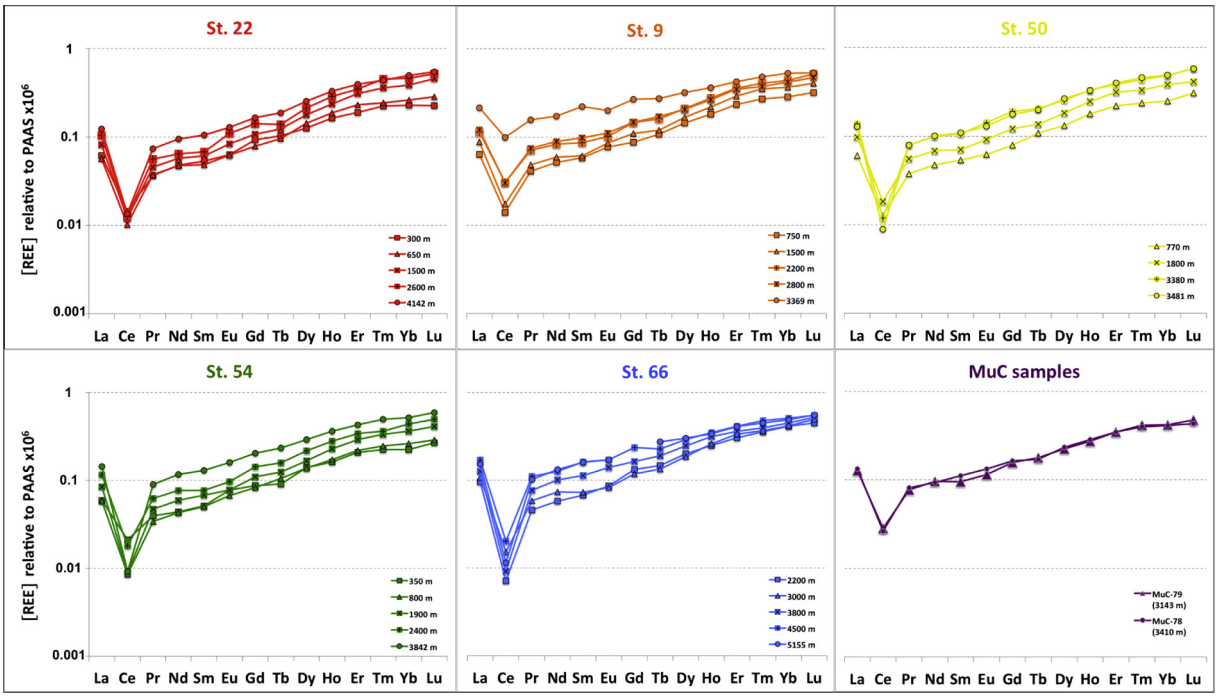

Fig. 4. Rare Earth Element (REE) patterns normalized to Post-Achaean Australian Sedimentary rocks (PAAS) (Taylor and McLennan, 1985) for the five CTD profiles and the two Multicorer seawater samples (MuC). From east to west: St. 22 (red), St. 9 (orange), St. 50 (yellow), St. 54 (green), St. 66 (blue) and MuC (purple). Note that Gd is missing in sample 66–5155. (For interpretation of the references to colour in this figure legend, the reader is referred to the web version of this article.)

depths. Between approximately 2000 and 3000 m depth, the increase in the concentrations is less pronounced for profiles 22 and 66. These two stations are influenced by north and equatorial Pacific-derived waters at this depth range, where Nd concentrations >30 pmol/kg are expected (Piepgras and Jacobsen, 1988; Amakawa et al., 2004, 2009). The fact that the observed concentrations are by 10–15 pmol/kg lower may indicate pronounced scavenging processes in the equatorial Pacific as discussed below (Section 4.2.1).

3.4. Nd isotope compositions

The Nd isotope compositions of the samples range from -10.3 ± 0.3 to -5.4 ± 0.4 ε_{Nd} units (Fig. 5, Table 1). Intermediate waters, the domain of AAIW and its precursor SAMW (300–1500 m depth) show a range of ε_{Nd} signatures between -7.5 ± 0.3 and -9.0 ± 0.3. Below the influence of AAIW the most radiogenic Nd isotope compositions where found in the easternmost part of the study area, where the influence of waters derived from the north is greater. This is particularly the case for station 22 (80°W), which is located close to the South American continent and includes the main core of NPDW yielding the most radiogenic signatures of this study at 1500 m ($\varepsilon_{Nd} = -5.4 \pm 0.4$) and 2600 m ($\varepsilon_{Nd} = -5.8 \pm 0.3$) water depth. NPDW was also sampled further west (95°W) at station 9 (1500 m water depth) and therefore was more diluted with a slightly less radiogenic Nd signature of -6.4 ± 0.3. Below that depth, profile 9 shows a trend towards unradiogenic values with depth (-6.8 ± 0.3 to -9.1 ± 0.3), progressively reaching the domain of waters of circumpolar origin that occupy the deep Southeast Pacific Basin (Fig. 1b to f). Similarly, the westernmost profile at station 66 (150°W) also shifts towards less radiogenic values with depth (-6.0 ± 0.2 at 2200 m to -8.3 ± 0.3 at 5155 m). In this case the hydrographic data suggest the most positive ε_{Nd} values coincide with the presence of SPGDW and the most negative ε_{Nd} signatures with the core of LCDW. The ε_{Nd} signal is constant at -8.3 ± 0.3 from 3800 m to the bottom, reflecting the latter water mass.

Profiles 50 and 54, located above the East Pacific Rise (120°W to 110°W), include UCDW samples at 1800 m (-8.3 ± 0.2) and 1900 m (-7.6 ± 0.2) respectively. These profiles exhibit isotopic variations tending to more radiogenic values with depth, from -8.8 ± 0.4 to -7.0 ± 0.3 for station 50 and from -7.9 ± 0.3 to -6.5 ± 0.2, for station 54.

The bottom water signatures measured for the two deep samples obtained from the multicorer waters off New Zealand are amongst the most negative ones of this study, yielding ε_{Nd} signatures of -9.0 ± 0.3 for sample MuC-78 (3410 m depth) and -10.3 ± 0.3 for sample MuC-79 (3143 m depth).

4. DISCUSSION

4.1. Advection and water mass mixing in relation to Nd isotopes and Nd concentrations

Comparing the Nd concentrations observed in the Southern Pacific water column presented in this study with available data from other ocean basins our vertical [Nd]

gradients are less pronounced than in the north Pacific and rather resemble Southern and Indian Ocean profiles (Lacan et al., 2012 and references therein) reflecting the larger influence of Circumpolar Current derived waters in our study area. This implies efficient vertical mixing in the water column of the Antarctic Circumpolar Current and confirms a major role of advection in controlling the distribution of REEs. The physical processes that govern the distribution of the different water masses are clearly reflected by their Nd isotope characteristics as discussed below.

4.1.1. AAIW

Stations 22, 9, 50, and 54 are located just north of the formation region of AAIW, which is represented by 6 samples from between 300 and 800 m water depth. The average ε_{Nd} signature of AAIW samples in this study is -8.2 ± 0.3, which matches the signatures previously obtained for this water mass in the Atlantic sector of the Southern Ocean (Stichel et al., 2012). Fig. 6 shows endmember mixing calculations between different water masses based on their ε_{Nd} and [Nd] signatures and it is evident that all intermediate depth samples correspond to almost pure AAIW and that admixture of NPDW at this depth is below 10%.

Station 22 shows the most radiogenic value of all AAIW samples at 300 m depth ($\varepsilon_{Nd} = -7.5 \pm 0.3$) and corresponds to an oxygen minimum (see Fig. 5) interpreted to be consequence of its location (80°W) within the extension of the poleward flow of the Peru–Chile Undercurrent, which transports oxygen depleted Equatorial SubSurface Water (ESSW) (Tsuchiya and Talley, 1999). A much more radiogenic dissolved Nd isotope signature of ESSW (-4.5 ± 0.5) was determined by Jeandel et al. (2013) at their station UPX (see Fig. 1a) near our station 22. Their location is, however, very close to the Chilean coast (~60 km) and was most likely strongly affected by boundary exchange with the nearby continent.

Fig. 7, summarizes all available data of dissolved Nd isotope compositions on a N–S transect along the pathway of modified NPDW in the eastern Pacific (see Section 4.1.2.). AAIW gradually loses its signature by mixing as it flows to the north, changing from -8.4 ± 0.4 in the Southern Ocean (Stichel et al., 2012) to -6.5 ± 0.5 at 32°S (St. EGY, from Jeandel et al., 2013). Above and below AAIW more radiogenic and oxygen poor equatorial waters prevail: Eastern South Pacific Intermediate Water (ESPIW): -5.4 ± 0.5 (St. EGY, Jeandel et al., 2013) and modified NPDW: -5.4 ± 0.4 (sample 22–1500, this study).

4.1.2. LCDW and NPDW

The only significant advection of deep waters filling the entire deep Pacific takes place in the Southwest Pacific Basin in the form of LCDW. This northward transport is mainly compensated by the mid-depth return flow of NPDW in the eastern South Pacific. These water masses are responsible for the main deep water volume transport in the region at some 13 Sverdrup (Sv) each (Kawabe and Fujio, 2010). They also present the largest differences in ε_{Nd} signatures between individual water masses (excluding the multicorer samples), as well as in hydrographic properties within the study area. The Nd isotope signatures of all samples below ~1400 m are compared with temperature and salinity (potential density) and oxygen concentrations in order to evaluate their conservative behavior in Fig. 8.

LCDW is characterized by high salinities and low temperatures (σ_θ range: 28.15–28.21 kg/m^3), as well as high oxygen content (4.2–4.4 ml/l) and occupies the deepest regions of the study area. Here we do not consider the multicorer samples (180°W) to be LCDW given that these

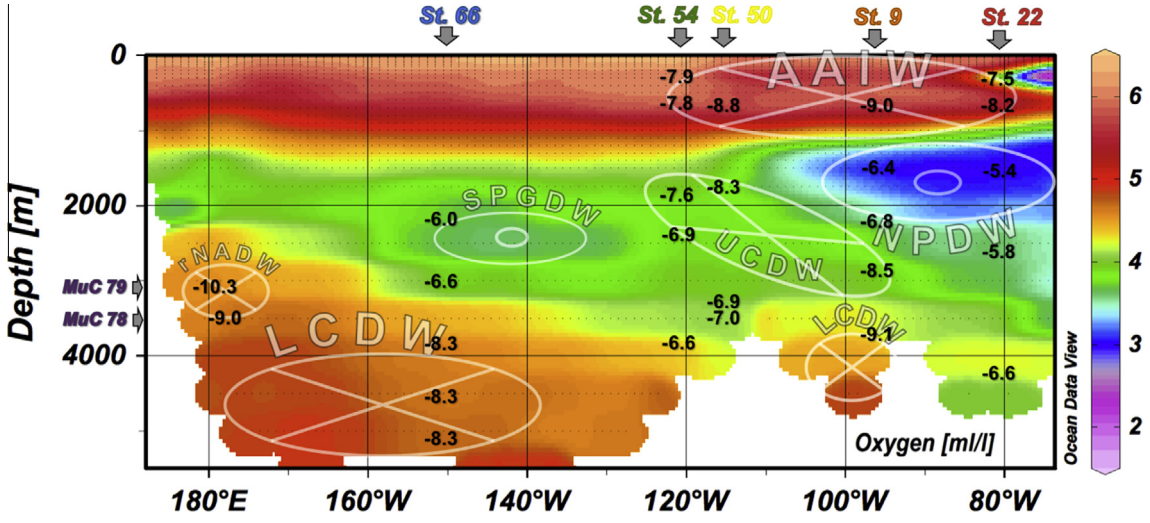

Fig. 5. Section (see Fig. 1a) of oxygen concentrations (ml/l) and measured ε_{Nd} signatures (black numbers) at their corresponding depths. The flow direction of the main water masses present in the study area are also shown by transparent circles, where crosses represent the sense of movement into the picture and centred circles represent movement out of the picture. Water mass abbreviations: LCDW (Lower Circumpolar Deep Water), rNADW (residual North Atlantic Deep Water), AAIW (Antarctic Intermediate Water), UCDW (Upper Circumpolar Deep Water), SPGDW (South Pacific Gyre derived Deep Water) and NPDW (North Pacific Deep Water). Oxygen concentrations were obtained from the World Ocean Atlas 09. (For interpretation of the references to colour in this figure legend, the reader is referred to the web version of this article.)

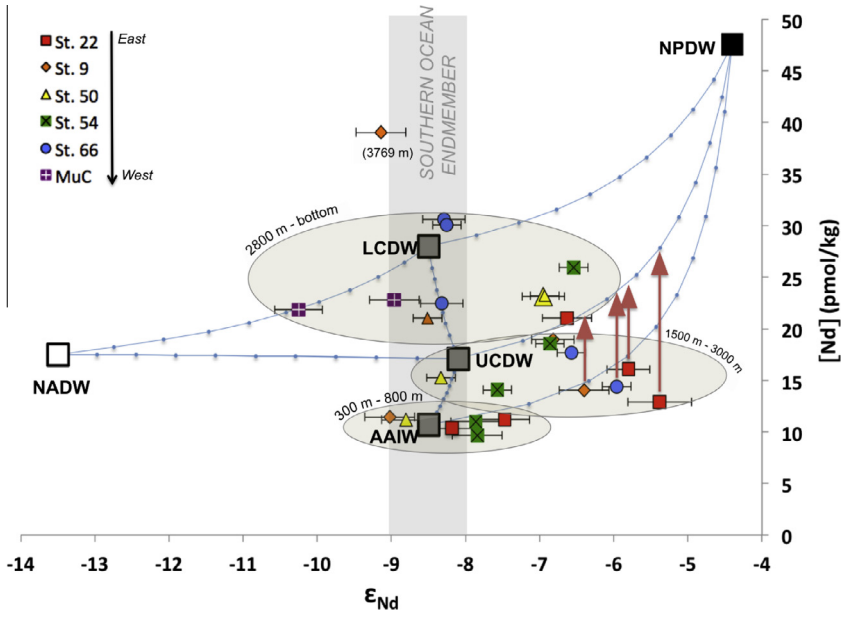

Fig. 6. Endmember mixing lines (blue) of Nd concentrations and isotope compositions between different water masses divided into 10% steps (blue dots). Large squares represent the endmembers, with those originating in the Southern Ocean marked by a grey bar. Symbols represent the results of this study, coded by stations. The results are grouped by ranges of water depth (grey circles). Red arrows illustrate the offset caused by scavenging on the samples located within NPDW and SPGDW (see section 4.3). The values of the endmembers correspond to [Nd] in pmol/kg and ε_{Nd} at their origins: NADW ([Nd] = 17.5, $\varepsilon_{Nd} = -13.5$, Piepgras and Wasserburg (1987)), LCDW ([Nd] = 28, $\varepsilon_{Nd} = -8.5$, Carter et al. (2012)), UCDW ([Nd] = 17.1, $\varepsilon_{Nd} = -8.1$, averaged from Carter et al. (2012) and Stichel et al. (2012)), AAIW ([Nd] = 10.7, $\varepsilon_{Nd} = -8.5$, averaged from Stichel et al. (2012) and this study) and NPDW ([Nd] = 47.6, $\varepsilon_{Nd} = -4.4$, averaged from the locations closest to the formation region of modified NPDW according to Kawabe and Fujio (2010) based on the results of Amakawa et al. (2009) and Piepgras and Jacobsen (1988)) Nd concentrations presented in this figure were obtained by the Isotope Dilution (ID) technique. (For interpretation of the references to colour in this figure legend, the reader is referred to the web version of this article.)

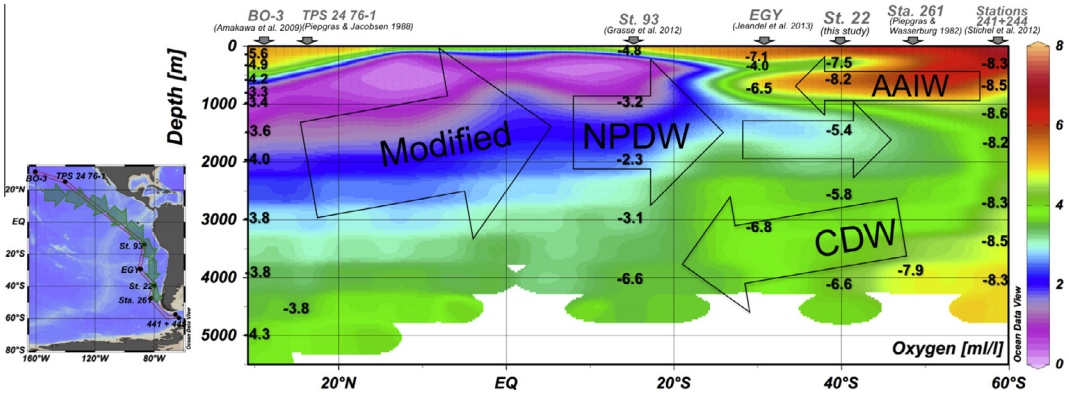

Fig. 7. North–South section along the flow path of modified NPDW after Kawabe and Fujio (2010) (green arrows on section), showing oxygen concentrations (ml/l), represented by the colour gradient, and ε_{Nd} signatures (black numbers) at their corresponding depths from this and other studies of seawater Nd isotope compositions of the Pacific Ocean. The flow direction of the main water masses are also shown by transparent arrows. Water mass abbreviations: CDW (Circumpolar Deep Water), AAIW (Antarctic Intermediate Water) and NPDW (North Pacific Deep Water). Oxygen concentrations were taken from the database of the World Ocean Atlas 09. (For interpretation of the references to colour in this figure legend, the reader is referred to the web version of this article.)

are clearly influenced by advection of North Atlantic derived waters (Section 4.1.3). Thus homogenized LCDW was sampled below 3500 m depth of profile 66 (150°W) with a constant ε_{Nd} signature of −8.3 (±0.3). This value is the same as found previously for pure LCDW in the Drake Passage (Piepgras and Wasserburg, 1982; Stichel et al., 2012) and is identical within uncertainties to the average ε_{Nd} value observed for the same water mass at the zero meridian in the Atlantic Sector of the Southern Ocean −8.7 (±0.4) (Stichel et al., 2012) and in the Bellingshausen and Amundsen seas −8.7 (±0.2) (Carter et al., 2012).

Apart from the main flow entering the Southwest Pacific basin, LCDW also occupies the bottom of the southeast Pacific basin (Fig. 1b–f) below 3000 m depth (Warren, 1973).

Although profile 9 (95°W) does not reach the deepest parts of this basin (see Fig. 8) and thus mainly represents shallower UCDW (Section 4.1.3), an influence of LCDW on the deepest sample of this station (9–3769) cannot be excluded. This sample has a Nd isotope composition of -9.1 ± 0.3, which points to the presence of circumpolar deep waters, although being slightly less radiogenic than typical signatures of LCDW in other basins. This sample has anomalously high LREE concentrations likely reflecting a significant sedimentary input (see Section 4.4.1). However, Nd isotope signatures of detrital components of South Pacific sediments in this region are more radiogenic at values >-5 (e.g. Jeandel et al., 2007, GEOROC database and references therein) suggesting the LREE enrichment does not originate from local detrital material.

NPDW is the second major water mass endmember below the influence of AAIW in the South Pacific. Based on the hydrographic data (σ_0: 27.60–28.00 kg/m^3, [O_2]: 2.6–3.3 ml/l), profiles 22 and 9, show the major influence of North Pacific derived waters within the study area between 1500 and 2600 m depth. This is also documented by their ε_{Nd} values, clearly marking the influence of radiogenic source waters from the North Pacific: -5.4 ± 0.4 and -5.8 ± 0.3 for station 22 at 1500 and 2600 m depth, respectively and -6.4 ± 0.3 for sample 9–1500.

Kawabe and Fujio (2010) described in detail the distribution of NPDW within the entire Pacific ocean and identified two characteristic types; one that occupies wide areas of the deep water column of the North Pacific and one that flows in a southeasterly direction from the central North Pacific to the Antarctic, which they named modified NPDW given that it experienced admixture of significant amounts of LCDW and UCDW. This modified version of NPDW flows to the east and then south adjacent to the American continents, passing our section at stations 22 and 9.

Amakawa et al. (2009) reported an average ε_{Nd} value of -3.9 ± 0.7 for pure NPDW using data from different studies of dissolved Nd isotope compositions in the North Pacific (Piepgras and Jacobsen, 1988; Amakawa et al., 2004, 2009). The ε_{Nd} signatures track the flow path of modified NPDW from the central Pacific to the Drake Passage (Fig. 7). Despite the coarse resolution of the data, in particular between 20°S and 20°N, a clear gradual trend to less radiogenic ε_{Nd} values from North to South can be observed in Fig. 7 with the exception of middepth waters at station 093 (Grasse et al., 2012) in the Eastern Equatorial Pacific (EEP). For this station, dissolution of particles of volcanic origin from South America was invoked as a cause for the signatures even more radiogenic than in the central North Pacific. On the other hand, between 30°S and 60°S (Fig. 7), CDW and AAIW become gradually more radiogenic (CDW evolving from -8.4 ± 0.4 in the Southern Ocean (Stichel et al., 2012) to -6.6 ± 0.3 at 14°S (St. 093; Grasse et al., 2012)) as they flow to the north sandwiching the remnants of modified NPDW (-5.4 ± 0.4). Horikawa et al. (2011) observed a similar Nd isotope evolution of NPDW along their eastern Pacific (EP) transect obtained from fish teeth in surface sediments.

Jeandel et al. (2013) tentatively attributed the more radiogenic Nd isotope signatures of their unfiltered samples

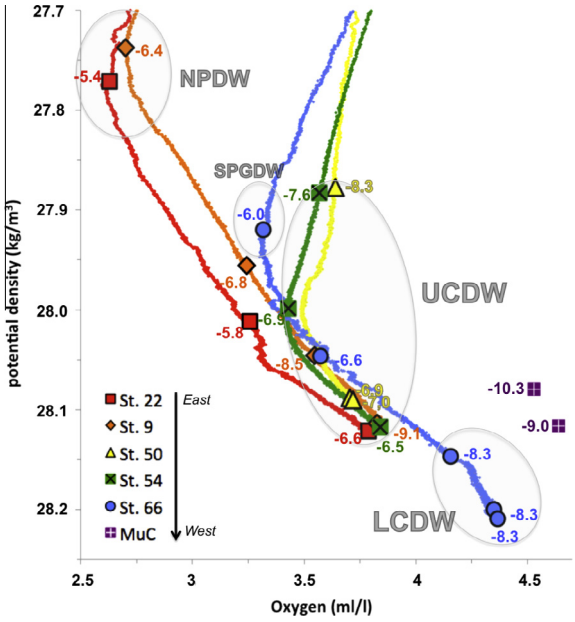

Fig. 8. Nd isotope compositions of all samples (symbols) below the influence of AAIW (~1400 m) together with potential density and oxygen concentrations from the five CTD profiles and the two multicorer water samples (MuC) of this study. Hydrographic data from the MuC samples was obtained from World Ocean Atlas 09. From east to west: St. 22 (red), St. 9 (orange), St. 50 (yellow), St. 54 (green), St. 66 (blue) and MuC (purple). The identified water masses are indicated by grey circles: NPDW (North Pacific Deep Water), SPGDW (South Pacific Gyre derived Deep Water), UCDW (Upper Circumpolar Deep Water) and LCDW (Lower Circumpolar Deep Water). (For interpretation of the references to colour in this figure legend, the reader is referred to the web version of this article.)

(-6.8 ± 0.8, -3.7 ± 0.7 and -5.2 ± 0.4) at middepths (2000–3200 m) to a potential hydrothermal contribution from the East Pacific Rise. Given the location of their stations GYR and EGY in the central and eastern South Pacific (see Figs. 1 and 7) and the evolution of modified NPDW along the flow path described above, admixture of NPDW provides an alternative explanation for their radiogenic values between 2000 and 3200 m depth. Further detailed investigations, such as in the frame of the planned GEOTRACES sections in the Pacific Ocean, are required to better characterize the evolution of NPDW in terms of Nd isotopes and to elucidate potential hydrothermal effects.

Kawabe and Fujio (2010) suggested that modified NPDW forms at 15–25°N, 155°W, where the average ε_{Nd} signature below 2000 m from Amakawa et al. (2009) and Piepgras and Jacobsen (1988) is −4.4 corresponding to a Nd concentration of 47.6 pmol/kg. Assuming these values as endmembers for modified NPDW, and taking into account the effect of LREE scavenging that occurs in the eastern equatorial Pacific (see Section 4.3), simple mixing calculations (Fig. 6) suggest that the fraction of NPDW still amounts to 30–50% at stations 22 and 9 located within the trajectory of this water mass. The remaining 50–70% consist of intermediate and middepth waters from the Southern Ocean (AAIW and UCDW).

The impact of the two major water masses (LCDW and NPDW) on the Nd isotope compositions and Nd concentrations in the South Pacific have been modeled (Rempfer et al., 2011). Simulated Nd isotope distributions covering our study area obtained from this model (Fig. 9a) predict the cores of both water masses roughly at the positions observed in this study, with simulated LCDW ($\varepsilon_{Nd} \sim -7$) dominating below 3000 m predominantly at the western end, and simulated NPDW ($\varepsilon_{Nd} \sim -4$) adjacent to South America occupying mid-depth waters. The absolute values obtained from the model are one to two ε_{Nd} units more radiogenic compared to observations, probably resulting from an overestimation of weathering or boundary exchange contributions from South America in the model.

4.1.3. UCDW, SPGDW, and NADW

Apart from the volumetrically most important water masses LCDW and NPDW, the presence and/or influence of three other water masses can be traced using Nd isotopes, namely: UCDW, SPGDW and NADW. These water masses are not captured in the modeled section of Fig. 9 due to the low resolution of the model.

Pure mid-depth circumpolar waters (UCDW) are difficult to identify in the South Pacific due to the predominance of Pacific-derived waters in the same depth range (see Section 1.1). Thus, UCDW can only be clearly identified based on its Nd isotope composition at (1) Station 9 located in the southeast Pacific basin where the deepest part is occupied by ACC-derived waters (Warren, 1973) (Fig. 5) and (2) above the East Pacific Rise sampled at stations 50 and 54 (Fig. 5), where the main inflow of UCDW into the Pacific takes place (Kawabe and Fujio, 2010). Sample 9-2800 shows a ε_{Nd} value of -8.5 ± 0.2. The presence of UCDW at these location and depth has been reported by Tsuchiya and Talley (1999) and can also be inferred from the low phosphate contents in Figs. 1e and 2b. Sample 9-3769 ($\varepsilon_{Nd} = -9.1 \pm 0.3$) is also under the influence of UCDW (Fig. 1b–f), and has a slightly less radiogenic signature than average CDW. Samples 50–1800 and 54–1900 reflect pure circumantarctic isotopic compositions of -8.3 ± 0.2 and -7.6 ± 0.2 respectively. The signatures of these samples located above the East Pacific Rise reflect the dominance of southern sourced mid-depth waters in this region over north and central Pacific sources. These observations are also in agreement with the ε_{Nd} measurements by Carter et al. (2012) (at their station 022 located 20° south of our study area (Fig. 1a) pure CDW averages -8.4 ± 0.3 ε_{Nd} units between 1500 and 3500 m).

Another example for the close correspondence of hydrological properties and Nd isotope signatures is the evolution of mid-depth waters of the central Pacific below the South Pacific Subtropical Gyre. In the Southwest Pacific basin between 1500 and 3000 m water depth, SPGDW is produced because the dynamics of the South Pacific Subtropical Gyre also affects the deeper water column. UCDW that enters the Pacific across the East Pacific Rise mixes with central Pacific middepth waters, and is then transported from the equator to the south causing mixed hydrographic properties between Antarctic-derived waters and NPDW (Reid, 1986). Sampled at St. 66 (150°W) at 2200 m, this water mass yields an ε_{Nd} value of -6.0 ± 0.2 and an oxygen concentration of 3.3 ml/l, more radiogenic and less oxygenated than samples obtained at the same depth further east where UCDW flows into the Pacific: St. 50 (Depth: 1800 m, $\varepsilon_{Nd} = -8.3 \pm 0.2$, $[O_2] = 3.6$ ml/l) and St. 54 (Depth: 1900 m, $\varepsilon_{Nd} = -7.6 \pm 0.2$, $[O_2] = 3.6$ ml/l).

The Nd isotopes also allow the detection of the influence that NADW exerts on circumpolar deep waters (Section 1.1). Residual NADW is still discernible in the western South Pacific at a depth near 3000 m between 180°E and 160°W by its salinity maximum, as well as low silicate and phosphate contents (Figs. 1c,e,f and 2b,c). Reid and Lynn (1971) tracked the pathway of this water mass by its oceanographic properties, passing our sampling location, into the North Pacific. Boundary exchange does not seem to significantly influence the Nd isotope compositions of our bottom water samples from New Zealand's Bounty Trough (MuC-78 and MuC-79) given that the ε_{Nd} values of New Zealand rocks range between -5 and $+1$ (Jeandel et al., 2007). Therefore, the unradiogenic values of

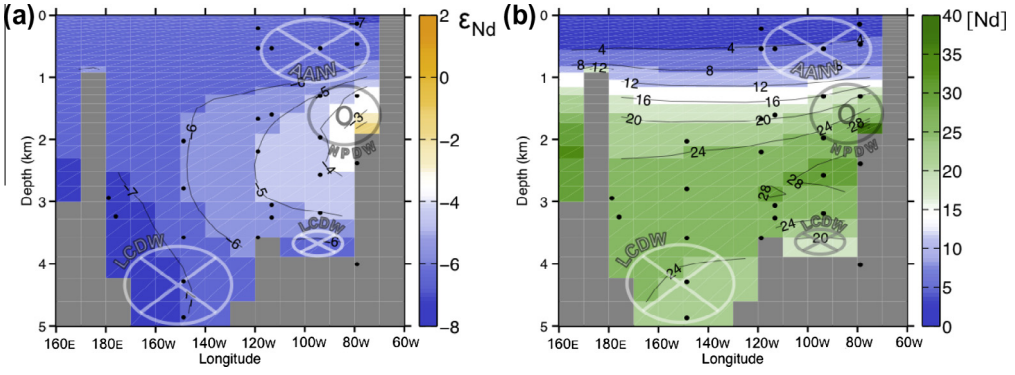

Fig. 9. Modeled Nd isotopic compositions (left panel) and Nd concentrations (right panel) from a transect located between 38°S and 42°S and the same longitude range as our study area (Rempfer et al., 2011). Figure provided by *J. Rempfer*. Black dots show the locations of the samples obtained in this study (see Fig. 5 for comparison). The flow direction of the water masses captured by the model are shown by transparent circles, where crosses represent the sense of movement into the picture and centred dots represent movement out of the picture. Water mass abbreviations: LCDW (Lower Circumpolar Deep Water), AAIW (Antarctic Intermediate Water) and NPDW (North Pacific Deep Water).

-9.0 ± 0.3 (MuC-78) and -10.3 ± 0.3 (MuC-79) reflect the advection of residual NADW. The difference of 1.3 ε_{Nd} units between these two samples may result from a larger fraction of this water mass present at the location of sample MuC-79, as inferred from its more negative ε_{Nd} value, as well as its lower nutrient concentrations and higher salinity (see Table 1 and Figs. 11e,f and 2b,c).

Fig. 6 indicates that sample MuC-79 ($\varepsilon_{Nd} = -10.25$, [Nd] = 21.8 pmol/kg), falls on the mixing line of LCDW and NADW, indicating mixing proportions of around 50% for the two water masses at 3100 m, 179°E, 45°S. Mixing proportions of LCDW and NADW using temperature and salinity at this station give a maximum of 25% of NADW indicating a stronger dilution of NADW along its flow path to the South Pacific than deduced from Nd isotope mixing calculations. The quantitative discrepancies most likely result from boundary exchange or reversible scavenging processes along the long flow path of NADW from its sources to this location.

4.1.4. Admixture of northern and southern derived middepth water masses

Apart from the distinct water masses described above, many of the samples of this study reflect mixing of waters of different hydrographic properties. Following potential density and oxygen concentrations (Fig. 8), all five profiles converge on the mixing line of NPDW and LCDW. UCDW samples of profile 9 also fall within this mix. making UCDW difficult to distinguish. Excluding the pure UCDW samples (Section 4.1.3), mixing between northern- and southern-derived waters is reflected by Nd isotope compositions ranging from -5.8 ± 0.3 to -7.0 ± 0.3 (Fig. 8). The endmember mixing calculations in Fig. 6 clearly indicate strong mixing between northern and southern sourced middepths waters for seven out of nine samples in the depth range of 1500–3000 m, although being depleted in Nd concentrations (see Section 4.3), yielding estimated NPDW contributions between 10% and 50%. The major influence of Pacific derived waters at middepths and of northward flowing Southern Ocean waters above and below deduced from hydrographic properties (Section 1.1), is also reflected in the Nd isotope compositions (Fig. 6), further supporting the use of Nd isotopes as a reliable water mass tracer in the open South Pacific.

4.2. Advective processes deduced from REEs

Further evidence for the quasi conservative behavior of REEs in the South Pacific can be inferred from the REE distributions. Normalization of the trivalent REEs to a reference water is a useful way to identify the distinct REE compositions of a particular water mass and provides important information on its origin as well as the oceanic processes that define it (e. g. Alibo and Nozaki, 2004). Regardless of the chosen reference water, the advantage over PAAS-normalized patters is that common features present in all seawater samples, such as the progressive enrichment from light to heavy REEs, are removed (Nozaki et al., 1999). The REE concentrations of NPDW sampled in the western North Pacific (34°N, 139°E) (Alibo and Nozaki, 1999) at around 2500 m depth have previously been used for normalization as these waters represent the oldest part of the global thermohaline circulation (Nozaki et al., 1999; Alibo and Nozaki, 2000, 2004; Nozaki, 2001; Nozaki and Alibo, 2003b).

Fig. 10 shows the NPDW normalized values for some water masses of this and other studies from the Southern Ocean and the western Pacific. All profiles of this study (Fig. 10a) are depleted compared to NPDW except samples collected from the main body of LCDW (indicated in orange in Fig. 10a). LCDW show a prominent LREE enrichment compared to the NPDW reference. Although in the case of sample 9–3369 a part of this effect may result from a bottom sedimentary source (see Section 4.4.1), a similar origin for this LREE enrichment is unlikely for the rest of the LCDW samples given that it is visible in the water column more than 1000 m above the bottom, therefore indicating this is a typical feature in the NPDW normalized pattern of LCDW. This LREE enrichment is also observed in deep samples from the Atlantic sector of the Southern Ocean at 39°S, 01°E (dashed brown lines in Fig. 10b; data from German et al., 1995). Nozaki and Alibo (2003b) suggested that AABW in low latitudes (40°S) close to its formation region, has undergone much less preferential scavenging of LREEs compared to older deep waters, therefore preserving its characteristic LREE enrichment with respect to NPDW.

In contrast, circumpolar deep waters from the Southeastern Indian Ocean exhibit MREE enrichments and strong depletions in LREE and Gd (dashed green lines in Fig. 10b), which, are thought to originate from admixture of southward flowing Indian Ocean deep waters affected by contributions from exchange with volcanic rocks of the Indonesian Archipelago, (Alibo and Nozaki, 2004). However, these Indian Ocean waters sampled at 40°S do not flow into the ACC and into the South Pacific Ocean where we have sampled for this study.

Samples influenced by North Pacific mid-depth waters of this study (indicated in blue in Fig. 10a) have a characteristic pattern with a relative LREE and MREE depletion: Pr to Eu depletion for SPGDW and Nd to Tb depletion for NPDW. This shape is consistent with samples from similar depths (dashed blue lines in Fig. 10b) in the Western South Pacific (27°S, 175°E) (Zhang and Nozaki, 1996; Alibo and Nozaki, 2004), indicating a pronounced homogeneity of waters of Pacific origin. These characteristic patterns reflect the preferential scavenging of LREEs and MREEs that these older water masses have undergone during advection from their source regions in the North and central Pacific (Section 4.3).

The South Pacific AAIW patterns observed here (red patterns in Fig. 10a) fall within the NPDW normalized patterns observed elsewhere but are more similar to those of the S. Atlantic than to the Indian Ocean waters. A distinct REE pattern of AAIW may prove useful for separating the northern and southern sourced Pacific intermediate waters that have similar hydrographic properties.

4.3. Biogeochemical cycling and the REE distribution

The primary productivity maximum at the equator seems to exert a considerable influence on the distribution

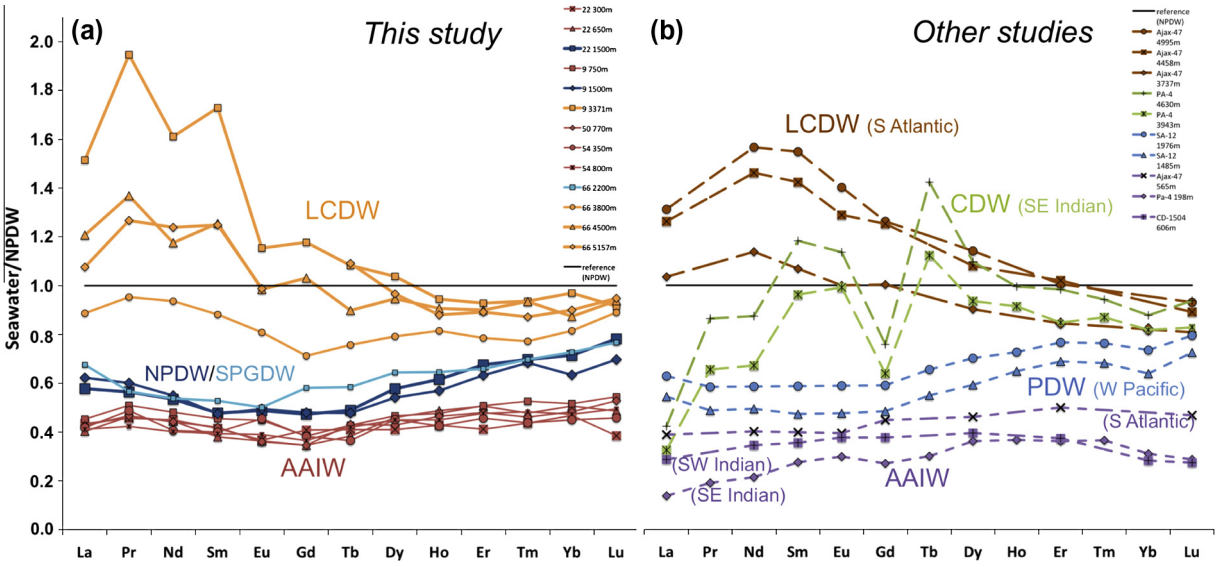

Fig. 10. NPDW-normalized patterns for selected samples of this study (left panel) and previous studies (dashed patterns in the right panel) from the South Atlantic (AJAX-47, German et al., 1995), the Southeastern Indian Ocean (PA-4, Alibo and Nozaki, 2004), the Southwestern Indian Ocean (CD-1504, Bertram and Elderfield, 1993) and the Western South Pacific (SA-12, Zhang and Nozaki, 1996) The different colours of the patterns reflect the dominance of a particular waters mass for each sample (indicated in the figure). NPDW reference concentrations after Alibo and Nozaki, 1999. Water mass abbreviations: LCDW (Lower Circumpolar Deep Water), AAIW (Antarctic Intermediate Water), CDW (Circumpolar Deep Waters) and PDW (Pacific Deep Water). (For interpretation of the references to colour in this figure legend, the reader is referred to the web version of this article.)

of REEs in our study area, which we will discuss using Nd concentrations as an example. Profiles 22 and 66 show small (4 to 5 pmol/kg) mid-depth depletions in Nd concentrations compared to the other stations (Fig. 3). This occurs exactly at depths where the influence of North Pacific-derived waters is largest (Sections 1.1. and 4.1). North Pacific waters have previously been shown to have the highest Nd concentrations in deep waters of all major ocean basins ranging between 40 and 50 pmol/kg (e.g. Lacan et al., 2012 and references therein). These high concentrations should therefore be traceable in our study area if [Nd] conservatively follows the advection of water masses from the north, as for example captured in the model of Rempfer et al. (2011). Their modeled South Pacific [Nd] section presented in Fig. 9b predicts concentrations of up to 28 pmol/kg between 2000 and 3000 m in the eastern part of our study area while we observe Nd concentrations ranging from 13 to 21 pmol/kg for these depths.

We suggest that the reason for the discrepancy between the model and the data is the southward advection of the middepth north Pacific water masses underneath the eastern equatorial high productivity area. The high rates of particle export will scavenge a significant amount of the dissolved Nd. This is consistent with the explanation of Grasse et al. (2012) for low concentrations in deep waters underneath the Peruvian upwelling area in the eastern equatorial Pacific. Jeandel et al. (2013) also observed unexpectedly low concentrations of 14.6–18.8 pmol/kg in the depth range of 2000–3000 m in the Southeast Pacific that they attributed to scavenging by metalliferous particles originating from hydrothermal vent fluids. Based on our findings the observations of Jeandel et al. (2013) may, however, also be explained by the advection of Nd depleted modified NPDW (see Section 4.1.2).

Scavenging processes especially affect the more particle reactive LREE, as reflected in the concentrations of La, Pr and Sm (Fig. 3), which are depleted similar to Nd in north Pacific derived middepths waters. The samples influenced by northern derived mid-depth waters also have the highest Er/Nd ratio at this depth level (Fig. 3), indicating depletion of LREEs. This is especially evident in profile 22 influenced by southward flowing NPDW and the upper part of profile 66, where SPGDW is present. In contrast, similarities between the profiles of dissolved silicate and HREEs (Bertram and Elderfield, 1993; Nozaki and Alibo, 2003a) have suggest the coupling of the HREEs to silicate cycling and diatom productivity (Akagi et al., 2011). This could also be the case in the South Pacific given that erbium (Er) and silicate concentrations appear to be well correlated ($R^2 = 0.85$) (Fig. 11), whereas the correlation with LREEs, such as Nd, is significantly weaker ($R^2 = 0.52$). Nevertheless, the positive intercept of both [Er] and [Nd] with [Si] and the weak correlation of all lanthanides with silicate below AAIW (red trend lines in Fig. 11) indicate that the life cycle of diatoms and dissolution of opal is not the main factor controlling the distribution of REEs in the South Pacific. This contrasts with the strong correlation ($R^2 = 0.87$) of silicate and [Nd] observed by Stichel et al. (2012) in the Atlantic sector of the Southern Ocean within the zone of high opal productivity (Sarmiento et al., 2007) and related dissolution processes.

4.4. Sediment–bottom water interactions

4.4.1. Release of REEs from the sediments of the Southeast Pacific Basin

In our study area, the only example of sedimentary input of REEs can be found in the bottom waters of the Southeast Pacific basin, where sample 9–3769 shows relatively high LREE concentrations (e.g. [Nd] = 39.1 pmol/kg)(Fig. 3). Without a considerable modification of the Nd isotope composition (-9.1 ± 0.3, slightly less radiogenic than expected for LCDW) this cannot be explained by boundary exchange (e.g. Lacan and Jeandel, 2005).

The NPDW-normalized patterns (Fig. 10) clearly reveal the strong enrichment of LREE compared to other CDW samples, suggesting a significant sedimentary contribution of LREE to bottom waters. The PAAS-normalized pattern of this sample also clearly differs from that of the rest of the samples (Fig. 4), although it still shows a LREE to HREE enrichment and the negative Ce anomaly (Fig. 3), typical for seawater. The shape of the PAAS-normalized pattern is more indicative of the release of REE from oxides in the sediments than a detrital silicate component that would produce a generally flatter REE pattern (Haley et al., 2004). In addition, the relatively unradiogenic Nd isotope signature of this water sample (-9.1 ± 0.3) precludes detrital (-2 to $+5$ for South America (Jeandel et al., 2007, GEOROC database and references therein)) and/or hydrothermal contributions. This suggests that although a significant sedimentary source of LREEs to the bottom water is identified at this location, probably the result of the sluggish circulation (Reid, 1997; Shaffer et al., 2004) caused by the barrier of the East Pacific Rise and Chile Rise that hinders equatorward deep water flow, this LREE enrichment from oxides does not alter the isotopic composition of bottom waters as the oxides are releasing LREEs previously scavenged from the same water mass. Evidence for REE release from sedimentary iron oxides within LCDW that did not influence the Nd isotopic composition has recently been suggested in an experimental study (Willson et al., 2013).

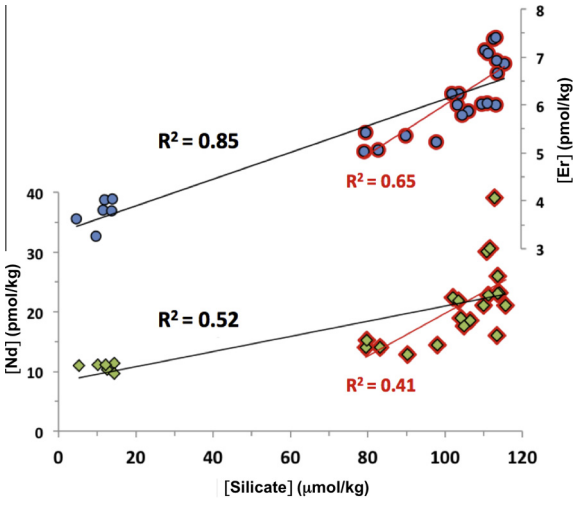

Fig. 11. Nd (green diamonds) and Er concentrations (blue dots) (pmol/kg) versus dissolved silicate concentrations (µmol/kg) and their respective correlation coefficients (R^2) for all samples (black trend line) and for samples below the influence of AAIW (~1400 m) (red contoured samples and linear fit). Nd concentrations presented in this figure were obtained by the Isotope Dilution (ID) technique. (For interpretation of the references to colour in this figure legend, the reader is referred to the web version of this article.)

4.4.2. Waters at the sediment–water interface

In contrast to the open ocean waters of this study, the bottom water samples from the Bounty Trough off New Zealand allow the evaluation of exchange processes between surface sediments and bottom waters from a slope setting located in the Deep Western Boundary Current (DWBC) of the South Pacific. The REE concentrations and PAAS-normalized REE patterns of the two multicorer seawater samples (MuC-78 and MuC-79) show a typical open ocean pattern (Figs. 3 and 4) indistinguishable from that of other samples of this study at similar depths. This suggests the absence of significant additions of sedimentary REEs to the bottom waters at this location. The only exception is Ce, which shows a slightly higher concentration (by 7–9 pmol/kg) that may point to a small sedimentary contribution of Ce to the bottom water.

Further confirmation of the absence of boundary exchange effects or input processes on our multicorer samples is obtained from the comparison between the dissolved Nd isotopic ratios of these two samples (-9.0 and -10.3) and the signatures of the detrital material supplied from New Zealand ($\varepsilon_{Nd} = -5$ to $+1$ (Jeandel et al., 2007)). Although only based on two samples from one location these results suggest insignificant sedimentary contributions to the REE budget of bottom waters located in the Deep Western Boundary Current (DWBC) of the South Pacific. This contrasts with the observations along the flow path of the DWBC in the Indian Ocean (Wilson et al., 2012) and also with boundary exchange processes observed along the South American margin (Grasse et al., 2012; Jeandel et al., 2013) and other regions of the Pacific (Horikawa et al., 2011), which may be explainable by different prevailing rock types of the detrital particles.

The absence of REE contributions from the surface sediments to the bottom water is consistent with the observations of Haley et al. (2004) who also used multicorers to collect waters directly overlying the sediment off Peru and in the California basin. Dedicated studies of the interaction processes between the seafloor and bottom waters in different environments are needed to further elucidate the mechanisms leading to "boundary exchange". This process has been demonstrated to play a crucial role in the global budget and distribution of the REEs in the oceans (Lacan and Jeandel, 2005; Arsouze et al., 2009; Rempfer et al., 2011; Wilson et al., 2012; Pearce et al., 2013) but clearly is regionally variable, most likely as a function of the lithologies of the sediments and may also vary with time.

5. CONCLUSIONS

The first analyses of dissolved Nd isotopes and REE concentrations in the intermediate to deep-water column

of the open mid-latitude South Pacific, overall confirm the reliability of Nd isotopes as water mass tracer in this region. Variations generally occur in correspondence with changes in hydrographic parameters, especially oxygen concentrations, which is the property that best distinguishes the Pacific water masses. The location and mixing of the different water masses could be tracked by combining Nd isotopes and hydrographic parameters: Pure circumpolar waters (AAIW and LCDW), occupying the shallowest and deepest areas of the analyzed depth range, respectively, reveal an ε_{Nd} signature of -8.3 ± 0.3, consistent with previous observations in the Atlantic and Pacific sectors of the Southern Ocean. Admixture of Pacific-derived waters partly replaces UCDW at middepths, except in isolated cases such as above the East Pacific Rise. Southward flowing Pacific derived waters are especially dominant at middepths of the eastern part of the study area, as well as in the Southwest Pacific basin where the main cores of NPDW and equatorial derived deep waters (SPGDW) are located and the most radiogenic ε_{Nd} values of -5.4 ± 0.4 and -6.0 ± 0.2 are found. The influence of residual NADW in the westernmost South Pacific is documented by the least radiogenic Nd isotopic signatures ($\varepsilon_{Nd} = -10.3 \pm 0.3$) and supported by low nutrient concentrations and high salinities. The Nd isotope distribution thus reliably fingerprints the most important water masses of the South Pacific and their mixtures, which will also serve as a basis for reconstructions of past deep water circulation using ε_{Nd} signatures extracted from marine sediments in this important region of the world's ocean.

The resemblance of NPDW-normalized REE patterns of LCDW samples of this study to those from the deep South Atlantic suggests a strong influence of AABW on CDW of the deep South Pacific and South Atlantic basins. Distinct NPDW-normalized REE patterns are also found for LCDW, NPDW and AAIW in the South Pacific.

Scavenging processes underneath the eastern equatorial high productivity area diminish the LREE concentrations of NPDW during its southward advection to the circumpolar region, producing non-conservative behavior of Nd concentrations. Local sedimentary input is only observed in bottom waters of the Southeast Pacific Basin by release of LREE from oxides in the sediments without modification of the Nd isotope composition. On the other hand, the analysis of waters from the sediment–water interface located under the influence of the South Pacific deep western boundary current off New Zealand does not provide evidence for significant boundary exchange or sedimentary REE input. This suggests that boundary exchange is spatially and temporally discontinuous and further studies from different regions and settings are required to quantify and better understand this process.

ACKNOWLEDGEMENTS

We would like to thank the "Bundesministerium für Bildung und Forschung, Germany" for funding this project (No.: 03G0213B), the crew members and participants of expedition SO213, in particular D. Nürnberg and R. Tiedemann for organizing and leading the cruise, which was part of the collaborative SOPATRA (SOuth PAcific paleoceanographic TRAnsect) project between the GEOMAR Helmholtz Centre for Ocean Research Kiel and the Alfred Wegener Institute for Polar and Marine Research (AWI) in Bremerhaven. R. Tiedemann (AWI) provided the nutrient data. We also thank J. Rempfer, University of Berne, for providing the modelled section of the study area and Jutta Heinze for laboratory assistance. Comments by the associate editor Mark Rehkämper, as well as by David Wilson and two anonymous reviewers improved the quality of this paper significantly.

REFERENCES

Akagi T., Fu F.-F., Hongo Y. and Takahashi K. (2011) Composition of rare earth elements in settling particles collected in the highly productive North Pacific Ocean and Bering Sea: implications for siliceous-matter dissolution kinetics and formation of two REE-enriched phases. *Geochim. Cosmochim. Acta* **75**, 4857–4876.

Alibo D. S. and Nozaki Y. (1999) Rare earth elements in seawater: Particle association, shale-normalization, and Ce oxidation. *Geochim. Cosmochim. Acta* **63**, 363–372.

Alibo D. S. and Nozaki Y. (2000) Dissolved rare earth elements in the South China Sea: geochemical characterization of the water masses. *J. Geophys. Res.* **105**, 28771–28783.

Alibo D. S. and Nozaki Y. (2004) Dissolved rare earth elements in the eastern Indian Ocean. *Deep-Sea Res. I* **51**, 559–576.

Amakawa H., Nozaki Y., Alibo D. S., Zhang J., Fukugawa K. and Nagai H. (2004) Neodymium isotopic variations in Northwest Pacific water. *Geochim. Cosmochim. Acta* **68**, 715–727.

Amakawa H., Sasaki K. and Ebihara M. (2009) Nd isotopic composition in the central North Pacific. *Geochim. Cosmochim. Acta* **73**(16), 4705–4719.

Arsouze T., Dutay J.-C., Lacan F. and Jeandel C. (2009) Reconstructing the Nd oceanic cycle using a coupled dynamical biogeochemical model. *Biogeosciences* **6**(12), 2829–2846.

Barrat J. A., Keller F., Amossé J., Taylor R. N., Nesbitt R. W. and Hirata T. (1996) Determination of rare earth elements in sixteen silicate reference samples by ICP-MS after Tm addition and ion exchange separation. *Geostand. Geoanal. Res.* **20**, 133–139.

Basak C., Martin E. E., Horikawa K. and Marchitto T. M. (2010) Southern Ocean source of 14C-depleted carbon in the North Pacific Ocean during the last deglaciation. *Nat. Geosci.* **3**(11), 770–773.

Bertram C. J. and Elderfield H. (1993) The geochemical balance of the rare earth elements and neodymium isotopes in the oceans. *Geochim. Cosmochim. Acta* **57**, 1957–1986.

Bostock H. C., Opdyke B. N. and Williams M. J. M. (2010) Characterising the intermediate depth waters of the Pacific Ocean using 13C and other geochemical tracers. *Deep-Sea Res. I* **57**, 847–859.

Byrne R. H. and Kim K. H. (1990) Rare earth elements scavenging in seawater. *Geochim. Cosmochim. Acta* **54**, 2645–2656.

Callahan J. E. (1972) The structure and circulation of deep water in the Antarctic. *Deep-Sea Res.* **19**, 563–575.

Carter P., Vance D., Hillenbrand C. D., Smith J. A. and Shoosmith D. R. (2012) The neodymium isotopic composition of waters masses in the eastern Pacific sector of the Southern Ocean. *Geochim. Cosmochim. Acta* **79**, 41–59.

Elderfield H. (1988) The oceanic chemistry of the rare-earth elements. *Philos. Trans. R. Soc. London, Ser. A* **325**, 105–126.

Elderfield H., Ferretti P., Greaves M., Crowhurst S., McCave I. N., Hodell D. and Piotrowski A. M. (2012) Evolution of ocean temperature and ice volume through the mid-pleistocene climate transition. *Science* **337**(6095), 704–709.

Frank M. (2002) Radiogenic isotopes: tracers of past ocean circulation and erosional input. *Rev. Geophys.* **40**, 1001.

German C. R., Masuzawa T., Greaves M. J., Elderfield H. and Edmond J. (1995) Dissolved rare earth elements in the Southern Ocean: cerium oxidation and the influence of hydrography. *Geochim. Cosmochim. Acta* **59**, 1551–1558.

Goldstein S. L. and Hemming S. R. (2003) Long-lived Isotopic Tracers in Oceanography. Paleoceanography, and Ice-sheet Dynamics, *Treatise on Geochemistry. Pergamon, Oxford.* pp. 453–489.

Grasse P., Stichel T., Stumpf R., Stramma L. and Frank M. (2012) The distribution of neodymium isotopes and concentrations in the Eastern Equatorial Pacific: water mass advection versus particle exchange. *Earth Planet. Sci. Lett.* **353–354**, 198–207.

Grasshoff K., Kremling K. and Ehrhardt M. (1999) *Methods of Seawater Analysis*. Verlag Chemie, Weinheim. pp. 159–228.

Grenier M., Jeandel C., Lacan F., Vance D., Venchiarutti C., Cros A. and Cravatte S. (2013) From the subtropics to the central equatorial Pacific Ocean: neodymium isotopic composition and rare earth element concentration variations. *J. Geophys. Res. Oceans* **118**, 1–27.

Haley B. A., Klinkhammer G. P. and McManus J. (2004) Rare earth elements in pore waters of marine sediments. *Geochim. Cosmochim. Acta* **68**, 1265–1279.

Hathorne E. C., Haley B. A., Stichel T., Grasse P., Zieringer M. and Frank M. (2012) Online preconcentration ICP-MS analysis of rare earth elements in seawater. *Geochem. Geophys. Geosyst.* **13**, Q01020. http://dx.doi.org/10.1029/2011GC003907.

Horikawa K., Martin E. E., Asahara Y. and Sagawa T. (2011) Limits on conservative behavior of Nd isotopes in seawater assessed from analysis of fish teeth from Pacific core tops. *Earth Planet. Sci. Lett.* **310**, 119–130.

Jacobsen S. B. and Wasserburg G. J. (1980) Sm–Nd isotopic evolution of chondrites. *Earth Planet. Sci. Lett.* **50**, 139–155.

Jeandel C., Arsouze T., Lacan F., Téchine P. and Dutay J.-C. (2007) Isotopic Nd compositions and concentrations of the lithogenic inputs into the ocean: a compilation, with an emphasis on the margins. *Chem. Geol.* **239**, 156–164.

Jeandel C., Delattre H., Grenier M., Pradoux C. and Lacan F. (2013) Rare earth element concentrations and Nd isotopes in the Southeast Pacific Ocean. *Geochem. Geophys. Geosyst.* **14**, 328–341. http://dx.doi.org/10.1029/GC004309.

Johannesson K. H. and Burdige D. J. (2007) Balancing the global oceanic neodymium budget: evaluating the role of groundwater. *Earth Planet. Sci. Lett.* **253**(1–2), 129–142.

Kawabe M. and Fujio S. (2010) Pacific Ocean circulation based on observation. *J. Oceanogr.* **66**, 389–403.

Lacan F. and Jeandel C. (2005) Neodymium isotopes as a new tool for quantifying exchange fluxes at the continent–ocean interface. *Earth Planet. Sci. Lett.* **232**, 245–257.

Lacan F., Tachikawa K. and Jeandel C. (2012) Neodymium isotopic composition of the oceans: a compilation of seawater data. *Chem. Geol.* **300–301**, 177–184.

Le Fevre B. and Pin C. (2005) A straightforward separation scheme for concomitant Lu–Hf and Sm–Nd isotope ratio and isotope dilution analysis. *Anal. Chim. Acta* **543**, 209–221.

Mantyla A. W. and Reid J. L. (1983) Abyssal characteristics of the World Ocean waters. *Deep-Sea Res.* **30**, 805–833.

Martin E. E., MacLeod K. G., Jiménez Berrocoso. A. and Bourbon E. (2012) Water mass circulation on Demerara Rise during the late Cretaceous based on Nd isotopes. *Earth Planet. Sci. Lett.* **327–328**, 111–120.

Moffet J. W. (1990) Microbially mediated cerium oxidation in sea water. *Nature* **345**, 421–423.

Noble T. L., Piotrowski A. M. and McCave I. N. (2013) Neodymium isotopic composition of intermediate and deep waters in the glacial southwest Pacific. *Earth Planet. Sci. Lett.* **384**, 27–36.

Nozaki Y. (2001) *Encyclopedia of Ocean Sciences* (eds. J. H. Steel et al.). Vol. 2, Academic Press. pp. 840–845.

Nozaki Y. and Alibo D. S. (2003a) Importance of vertical geochemical processes in controlling the oceanic profiles of dissolved rare earth elements inferred from the study in the northeastern Indian Ocean. *Earth Planet. Sci. Lett.* **205**, 155–172.

Nozaki Y. and Alibo D. S. (2003b) Dissolved rare earth elements in the Southern Ocean, southwest of Australia: unique patterns compared to the South Atlantic data. *Geochem. J.* **37**, 47–62.

Nozaki Y., Alibo D.-S., Amakwa H., Gamo T. and Hasumoto H. (1999) Dissolved rare earth elements and hydrography in the Sulu Sea. *Geochim. Cosmochim. Acta* **15**, 2171–2181.

Orsi A. H., Johnson G. C. and Bullister J. L. (1999) Circulation, mixing, and production of Antarctic Bottom Water. *Prog. Oceanogr.* **43**, 55–109.

Pahnke K., Goldstein S. L. and Hemming S. R. (2008) Abrupt changes in Antarctic intermediate water circulation over the past 25,000 years. *Nat. Geosci.* **1**, 870–874.

Pearce C. R., Jones M. T., Oelkers E. H., Pradoux C. and Jeandel C. (2013) The effect of particulate dissolution on the neodymium (Nd) isotope and rare earth element (REE) composition of seawater. *Earth Planet. Sci. Lett.* **369–370**, 21–40.

Piepgras D. J. and Jacobsen S. B. (1988) The isotopic composition of neodymium in the North Pacific. *Geochim. Cosmochim. Acta* **52**, 1373–1381.

Piepgras D. J. and Jacobsen S. B. (1992) The behavior of rare earth elements in the seawater: precise determination of variations in the North Pacific water column. *Geochim. Cosmochim. Acta* **56**, 1851–1862.

Piepgras D. J. and Wasserburg G. J. (1982) Isotopic composition of neodymium in waters from the Drake Passage. *Science* **217**, 207–214.

Piepgras D. J. and Wasserburg G. J. (1987) Rare earth element transport in the western North Atlantic inferred from Nd isotopic observations. *Geochim. Cosmochim. Acta* **51**, 1257–1271.

Piotrowski A. M., Galy A., Nicholl J. A. L., Roberts N., Wilson D. J., Clegg J. A. and Yu J. (2012) Reconstructing deglacial North and South Atlantic deep water sourcing using foraminiferal Nd isotopes. Earth Planet. *Sci. Lett.* **357–358**, 289–297.

Reid J. L. (1973) Transpacific hydrographic sections at Lats. 43°S and 28°S: the SCORPIO Expedition-III. Upper water and a note on southward flow at mid-depth. *Deep-Sea Res.* **20**, 39–49.

Reid J. L. (1986) On the total geostrophic circulation of the South Pacific Ocean: flow patterns, tracers and Transports. *Prog. Oceanog.* **16**, 1–61.

Reid J. L. (1997) On the total geostrophic circulation of the Pacific Ocean: flow patterns, tracers and transports. *Prog. Oceanog.* **39**, 263–352.

Reid J. L. and Lynn R. J. (1971) On the influence of the Norwegian-Greenland and Weddell seas upon the bottom waters of the Indian and Pacific oceans. *Deep-Sea Res.* **18**, 1063–1088.

Reid J. Ju, Stommel H., Dixon Stroup. E. and Warren B. (1968) Detection of a deep boundary current on the Western South Pacific. *Nature* **217**, 937.

Rempfer J., Stocker T. F., Joos F., Dutay J.-C. and Sidall M. (2011) Modelling Nd-isotopes with a coarse resolution ocean circulation model: sensitivities to model parameters and source/sink distributions. *Geochim. Cosmochim. Acta* **75**, 5927–5950.

Rickli J., Frank M. and Halliday A. N. (2009) The hafnium–neodymium isotopic composition of Atlantic seawater. *Earth Planet. Sci. Lett.* **280**, 118–127.

Roberts N. L., Piotrowski A. M., McManus J. F. and Keigwin L. D. (2010) Synchronous deglacial overturning and water mass source changes. *Science* **327**, 75.

Sarmiento J. L., Simeon J., Gnanadesikan A., Gruber N., Key R. M. and Schlitzer R. (2007) Deep ocean biogeochemistry of silicic acid and nitrate. *Global Biogeochem. Cycles* **21**. http://dx.doi.org/10.1029/2006GB002720.

Scher H. D. and Martin E. E. (2004) Circulation in the Southern Ocean during the Paleogene inferred from neodymium isotopes. *Earth Planet. Sci. Lett.* **228**, 391–405.

Shaffer G., Hormazabal S., Pizarro O. and Ramos M. (2004) Cirulation and variability in the Chile basin. *Deep-Sea Res. I* **51**, 1367–1386.

Siddall M., Khatiwala S., van de Flierdt T., Jones K., Goldstein S. L., Hemming S. and Anderson R. F. (2008) Towards explaining the Nd paradox using reversible scavenging in an ocean general circulation model. *Earth Planet. Sci. Lett.* **274**, 448–461.

Singh S. P., Singh S. K., Goswami V., Bhushan R. and Rai V. K. (2012) Spatial distribution of dissolved neodymium and ε_{Nd} in the Bay of Bengal: role of particulate matter and mixing of water masses. *Geochim. Cosmochim. Acta* **94**, 38–56.

Sloyan B. M. and Rintoul S. R. (2001) Circulation, renewal, and modification of Antarctic mode and intermediate water. *J. Phys. Oceanogr.* **31**, 1005–1030.

Stichel T., Frank M., Rickli J. and Haley B. A. (2012) The hafnium and neodymium isotope composition of seawater in the Atlantic sector of the Southern Ocean. *Earth Planet. Sci. Lett.* **317–318**, 282–294.

Stommel H. and Arons A. B. (1960) On the abyssal circulation of the world ocean—I. Stationary planetary flow patterns on a sphere. *Deep-Sea Res.* **6**, 140–154.

Stommel H., Dixon Stroup. E., Reid J. L. and Warren B. (1973) Transpacific hydrographic sections at Lats. 43°S and 28°S: the SCORPIO expedition–I. Preface*. *Deep-Sea Res.* **20**, 1–7.

Tachikawa K., Athias V. and Jeandel C. (2003) Neodymium budget in the modern ocean and paleo-oceanographic implications. *J. Geoph. Res.* **108** (C8).

Tanaka T., Togashi S., Kamioka H., Amakawa H., Kagami H., Hamamoto T., Yuhara M., Orihasi Y., Yoneda S., Shimizu H., Kunimaru T., Takahashi K., Yanagi T., Nakano T., Fujimaki H., Shinjo R., Asahara Y., Tanimizu M. and Dragusanu C. (2000) JNdi-1: a neodymium isotopic reference in consistency with LaJolla neodymium. *Chem. Geol.* **168**, 279–281.

Taylor, S. R., McLennan, S. M. 1985. The Continental Crust: Its Composition and Evolution. An Examination of the Geochemical Record Preserved in Sedimentary Rocks. Blackwell.

Tsimplis M. N., Bacon S. and Bryden H. L. (1998) The circulation of the subtropical South Pacific derived from hydrographic data. *J. Geophys. Res.* **103**, 21443–21468.

Tsuchiya M. and Talley L. D. (1996) Water-property distributions along an eastern Pacific hydrographic section at 135W. *J. Mar. Res.* **54**, 541–563.

Tsuchiya M. and Talley L. D. (1999) A Pacific hydrographic section at 88°W: water-property distribution. *J. Geophys. Res.* **103**, 12899–12918.

van de Flierdt T. et al. (2012) GEOTRACES intercalibration of neodymium isotopes and rare earth element concentrations in seawater and suspended particles. Part 1: reproducibility of results for the international intercomparison. *Limnol. Oceanogr.* **10**, 234–251.

Warren B. A. (1973) Transpacific hydrographic sections at Lats. 43°S and 28°S: the SCORPIO Expedition-II. Deep water. *Deep-Sea Res.* **20**, 9–38.

Wijffels S. E. (2001) Revisiting the South Pacific subtropical circulation: a synthesis of World Ocean circulation experiment observations along 32°S. *J. Geophys. Res.* **106**, 19481–19513.

Wilson D. J., Piotrowski A. M., Galy A. and McCave I. N. (2012) A boundary exchange influence on deglacial neodymium isotope records from the deep western Indian Ocean. *Earth Planet. Sci. Lett.* **341–344**, 35–47.

Wilson D. J., Piotrowski A. M., Galy A. and Clegg J. A. (2013) Reactivity of neodymium carriers in deep sea sediments: implications for boundary exchange an paleoceanography. *Geochim. Cosmochim. Acta* **109**, 197–221.

Zhang J. and Nozaki Y. (1996) Rare earth elements and yttrium in seawater: ICP-MS determinations in the East Caroline, Coral Sea, and South Fiji basins of the western South Pacific Ocean. *Geochim. Cosmochim. Acta* **60**, 4631–4644.

Associate editor: Mark Rehkamper